JOINT INSTITUTE FOR AERONAUTICS AND ACOUSTICS

National Aeronautics and Space Administration

Ames Research Center

Stanford University

JIAA TR-71

EXPERIMENTAL RESULTS OF THE CONTROL OF A VORTICAL FLOW BY TANGENTIAL BLOWING

N.J. Wood and L. Roberts

STANFORD UNIVERSITY

Department of Aeronautics and Astronautics
Stanford, California 94305

May 1986

Sep flow Control / Vortex flow

EXPERIMENTAL RESULTS ON THE CONTROL OF A VORTICAL FLOW BY TANGENTIAL BLOWING

N.J. Wood and L. Roberts
Joint Institute for Aeronautics and Acoustics
Dept of Aeronautics and Astronautics
Stanford University

JIAA TR-71

May, 1986.

ABSTRACT

This report documents the results of a wind tunnel test to investigate the controlling effects of tangential, leading edge blowing on the vortical flow over a delta wing. The blowing is used to directly control the cross-flow separation points at the rounded leading edge and hence, the trajectory of the feeding sheet and the location of the vortex. Experiments were conducted for both co-flowing and counter-flowing configurations over a range of angles of attack from 0 to 90 degrees. Results in the form of pressure distributions, overall force coefficients and flow mappings were obtained. The emphasis of this report is on data presentation rather than detailed analysis, that will be covered by subsequent documents.

The initial results indicate that the co-flowing configuration was capable of extending the regime of stable, controlled vortical flow over the upper surface by approximately 30 degrees angle of attack for modest blowing requirements. Increases in maximum normal force coefficient of approximately 30% were achieved and significant rolling moments produced at angles of attack from 30 to 60 degrees. The counter-flowing configuration indicated only minor lift augmentation with the exception of an isolated occurrence at 20 degrees angle of attack. At that condition, with very weak blowing, a lift augmentation, $(\partial C_N/\partial C_\mu)$ of approximately 20 was measured.

NOMENCLATURE

b	wing semi-span
c	wing root chord
C_n	spanwise sectional normal force coefficient
C_N	wing normal force coefficient
C_p	pressure coefficient
C_ℓ	spanwise sectional rolling moment coefficient
C_L	wing rolling moment coefficent
C_μ	blowing momentum coefficient
h	slot height
V_j	jet velocity
V_∞	free stream velocity
x,y	cartesian coordinates longitudinal and spanwise
α	angle of attack

TABLE OF CONTENTS

ABSTRACT i

NOMENCLATURE ii

1. INTRODUCTION 1

2. APPARATUS 3

2.1 Wind Tunnel 3

2.2 Delta Wing Model 3

2.3 Instrumentation 5

3. RESULTS 7

4. DISCUSSION 9

5. CONCLUSIONS 11

REFERENCES 12

TABLES AND FIGURES 13

1. INTRODUCTION

In recent years, it has become desirable to increase the angle of attack envelope of delta wing aircraft as a mechanism for improvement of their maneuverability[1]. Such vehicles rely on the development of strong, stable vortices over the upper surface of the wings to enhance their lifting capability. Typically these vortices may account for as much as 30% of the total vehicle lift and they become more important as the angle of attack increases beyond the range of operation of conventional wing systems. At these extreme angles of attack, certain phenomena such as vortex breakdown and asymmetric shedding may produce large periodic excursions in both the lift and rolling moments produced by the delta wing[2]. Naturally these phenomena are undesirable not only from a control aspect but also from structural and pilot safety considerations.

Some attempt has been made to provide active control of these large over-wing vortices through the use of controllable leading edge flaps[3,4]. These devices appear capable of improving the lift:drag ratio of a given wing, primarily through a drag reduction, but produce only modest improvements in the angle of attack envelope. Many attempts have also been made to control the trajectory and evolution of these vortices through spanwise blowing[5]. Either an injection of high momentum fluid into the core of the vortex or the ejection of a thin, high velocity fluid sheet beneath the vortical flow, is used. In some instances, the breakdown of the vortical flow has been successfully delayed and small increases in the angle of attack to stall have been obtained. Many of these techniques rely upon a direct interaction of the device with the global flowfield which results in a relatively

inefficient inviscid interaction.

The concept of Circulation Control on two-dimensional airfoils has been shown to be a strong viscous interaction which results in large changes in the global inviscid flowfield[6]. This concept utilizes a thin, high velocity, tangential jet of fluid to control the location of the rear separation points on a rounded trailing edged airfoil. Gains in lift coefficient of the order of 80 times the momentum injection have been observed over a wide range of operational conditions. The possibility then exists to consider the use of the Circulation Control concept as a crossflow plane device to directly control the location of the crossflow separation points and hence the trajectory of the ensuing vortices, figure 1. This of course requires the cross section of a delta wing to have rounded leading edges in contrast to the usual sharp configurations. To examine the practicality of such a scheme, a wind tunnel experiment has been performed to examine the lifting characteristics of a conical delta wing with tangential leading edge blowing. This report documents the initial results of the experimental study including some details of the model geometry, test conditions, pressure distributions and some initial flow mapping surveys in the crossflow plane.

2. APPARATUS

2.1 Wind Tunnel

The experiments were performed in the 18"x18" test section of the Stanford Low Speed Wind Tunnel. The tunnel has a maximum centerline free stream speed of 57m/s and is capable of continuous operation. Speeds in the range of 20 to 40 m/s were used throughout this experiment and this variation provided a mechanism for expansion of the range of blowing momentum coefficients that were achievable. Centerline velocities were monitored through a reference static pressure difference from two stations in the contraction which had previously been calibrated against a pitot static tube and shown to be free of interference due to the presence of the model.

A continuous operation centrifugal flow compressor was used as the source of compressed air for the blowing. This compressor is capable of delivering a maximum of 450 cfm at approximately 2 psi. The mass flow supplied to the model was measured from an in-line venturi meter and by direct measurement of the model internal pressure.

The model was mounted on a rotatable plate in the floor of the test section. Variations of the angle of attack of the model was obtained by rotation of the mounting plate to pre-determined locations. The model was mounted off-set from the center of rotation so as to minimize the blockage effects of the wing at high angles of attack.

2.2 Delta Wing Model

To simplify the comparison of the test results with theoretical predictions, it was required that the model be as near conical as possible

within the limits of practicality. This suggests that not only should the exterior be conical but also the internal plenum, and that the blowing slot height should vary linearly from the apex. Care should also be given to the arrangement of a satisfactory jet contraction with the jet exiting as near tangential as possible to the wing surface. These strict limitations led to a design scheme which was dictated by the limitations of the manufacturing capability at Stanford and the construction techniques that were available.

The overall dimensions of the wing were fixed to produce a 60 degree leading edge sweep angle and a root chord of 11 inches. A semi-span configuration was chosen to allow the scale of the model to be increased (relative to a full span model) and to simplify the ducting required for the blowing air supply.

The requirement for the internal geometry to be conical limited the design severely. To maintain this requirement, the leading edge of the wing was chosen to be a 4 degree half angle right circular cone whose axis was offset 26 degrees from the model centerline. Two flat plates were chosen to fabricate the remaining upper and lower surfaces of the wing and a cross section normal to the tunnel wall was defined to have parallel upper and lower surfaces. These few simple assumptions permitted the entire wing geometry (except the blowing slot) including skin thickness and leading edge cone tangency points to be defined.

To define the slot geometry, the slot was designed to be manufactured from two pieces. First a slot lip was detailed to be constructed by cutting two offset 4 degree half-angle conic cylinders to form a crescent. This could then be reduced to the required arc length to attach to the upper surface plate. The lower surface of the slot was produced from a 3 degree

half angle right circular cone whose axis had been carefully offset to produce the required slot height to span ratio while maintaining tangency with the lower surface. For simplicity the slot was not extended over the entire length of the leading edge. At the apex of the wing the geometry would have been impractical and at the trailing edge, a short length was allowed to facilitate the removal of the tubing attached to the pressure tappings without incurring air leaks from the internal plenum. Figure 2 illustrates the final model design.

To measure the loads on the wing a total of 189 pressure tappings were installed on the surfaces of the model in eight separate rows. At each row the tappings were placed on identical conical generators to simplify the data reduction. Table 1 gives a full listing of all the tapping locations. A single tapping was placed inside the model to permit measurement of the internal pressure. All of the 0.032" tubing used for the pressure tappings was carefully laid out on the inside surfaces of the plenum chamber and secured with adhesive. Care was taken to minimize the effect of the tubes upon the overall internal geometry. The tubes were routed through a bulkhead which was positioned at the trailing edge extent of the blowing slot and the plenum was carefully sealed at that point.

The co-flowing configuration is defined as that where the jet issues towards the upper surface i.e. co-flowing with the cross flow. The counter-flowing configuration is defined as the opposite.

2.3 Instrumentation

The pressure tappings in the model were monitored by a 4 barrel, 48 port Scanivalve pressure measuring system that was controlled by a PDP - 11/23

mini-computer. The Scanivalve was equipped with 4 +/- 2.5 psid pressure transducers that were conditioned to give 10 volts response per 1 psi of pressure. The data was sampled automatically, ensemble averaged and converted to pressure coefficient form for integration. Graphical displays of the individual spanwise pressure distributions was available on-line.

A five hole probe was used to obtain flow vector measurements in the cross-flow plane[7]. The probe was mounted on a 3-axis traversing gear which could be programmed to map out a predetermined orthogonal grid across the flow field. The calibration tables of the probe were stored on the same mini-computer and an efficient algorithm used such that real time display of the measured vectors could be produced.

3. RESULTS

The loads on the model were derived from integrations of the pressure distributions across the individual spanwise locations assuming a unit span at each location.

$$C_n = \int_0^1 C_p \, d(y/b)$$

A second integration was then performed between rows 2 and 7 to evaluate a wing loading coefficient. Account was taken of the change in dimension of the span at each row in order to produce a quasi conical normal force coefficient.

$$C_N = \frac{\int_{x_1}^{x_2} C_n . b \, dx}{\int_{x_1}^{x_2} b \, dx}$$

Rolling moments were calculated for each spanwise row and the rolling moment due to blowing found by subtraction of the unblown result for each angle of attack. It was assumed that the increment in rolling moment represented the full three-dimensional case and that no modification of the opposite wing span vortex flowfield resulted.

The blowing momentum coefficient for a conical blown delta wing is defined as follows

$$C_\mu = 2. \frac{V_j^2}{V_\infty^2} . \frac{h}{b}$$

The jet velocity was determined from the measurement of the internal

pressure of the model and the isentropic flow equations. The value of the slot height to span ratio was measured to be 0.0046 based on twice the span of the half model.

Figure 3 shows the normal force coefficient generated by the wing as a function of angle of attack without blowing. Figures 4 and 5 illustrate the longitudinal distribution of the normal force without blowing, for both configurations and figures 6 - 11 show some examples of the corresponding static pressure distributions.

Figure 12 shows the variation of the spanwise normal force coefficients for the co-flowing configuration and figures 13 - 20 show the associated static pressure distributions. Figures 21 and 22 - 24 display the equivalent results for the counter-flowing configuration. Figures 25 and 26 show the normal force and increment in rolling moment in the presence of blowing for the co-flowing configuration. Figure 27 shows the increments in normal force measured for the counter-flowing configuration. Figure 28 illustrates the measured effects of different Reynolds numbers on the production of wing normal force by blowing for the co-flowing configuration. Figures 29-31 show pressure contours deduced from the previously shown pressure distributions for some cases of interest in the co-flowing configuration. Figure 32 illustrates the blowing momentum boundary to achieve stable vortical flow as a function of increasing angle of attack.

The results of some cross-flow plane velocity measurements from the 5-hole probe system are shown in figures 33 - 36. These correspond to two mappings in the co-flowing configuration and two in the counter-flowing configuration. In either case, both a blown and an unblown condition is illustrated.

4. DISCUSSION

The unblown performance of this relatively thick delta wing configuration appears to exhibit quite reasonable trends in terms of the measured normal force coefficients, figure 3. The axial load distributions do however indicate that the flow over the wing at angles of attack in excess of 15 degrees does not appear to follow the expected conical trends. Indeed there is a pronounced decrease in the loads carried towards the trailing edge of the wing. This may be partly accounted for by the thickness of the wing as compared to the usual thin, slender delta approximation or it may well be that the rounded leading edge is producing a non-conical primary separation condition. A further condition of possible significance is a vortex burst phenomenon that may be moving towards the wing apex as angle of attack was increased. Such a phenomenon may cause the observed lack of conicality and its occurrence agrees with previous data for 60 degree swept delta wings. The large leading edge radius of the delta wing may be responsible for producing a very 'mild' vortex burst such that only moderate changes in normal force coefficients are observed. The generation of the normal force coefficient appeared to be quite symmetrical about the zero degree condition indicating that the presence of the slot was not unduly affecting the location of the primary separation.

A brief examination of the results in the presence of slot blowing clearly shows the significant control effected upon the vortical flow by the co-flowing configuration at extreme angles of attack. The introduction of the thin jet sheet around the leading edge of the wing has delayed the separation of the shear layer from the wing surface and moved the resulting vortex

closer to the wing surface. Consequently, stable attached flow can be observed to be present at angles of attack of at least 60 degrees. This effect is most clearly visible in the flow mappings given as figures 32 and 33. The areas around the core of the vortex were not mapped due to limitations of the calibration range of the 5-hole probe. It is interesting to note the strong generation of rolling moment also produced above the unblown stall angle of attack, figure 26. This suggests the possibility not only for discrete flow stabilization but also for the control of moment perturbations generated by flow asymmetries at high angles of attack or during rapid maneuvers. The fact that the flow control is capable of re-establishing the stable vortex flowfield suggests that the moments produced should at least be equivalent to those produced as a result of asymmetric vortex shedding.

Conceptually, the phenomenon observed for the co-flowing configuration may be considered to be equivalent to a de-coupling of the linear and non-linear lift contributions. As the co-flowing blowing is introduced the linear or attached flow contribution remains almost constant and a function of angle of attack. The non-linear or vortex lift contribution takes on a value which corresponds to a lower angle of attack (hence the vortex stabilization) which when combined with the linear contribution results in a positive increment in normal force.

The contours of constant pressure coefficient given in figures 28 - 30 clearly show the re-establishment of the vortical flow. The comparison for the 40 degree blown case and the 30 degree unblown case is quite striking, further evidence of the de-coupling of the two lift components and the degree of control produced by the co-flowing configuration.

5. CONCLUSIONS

A preliminary wind tunnel test has been successfully completed on a delta wing with tangential leading edge blowing. Initial results indicate an improvement of 30 degrees in the angle of attack range of the wing for stable vortical flow depending on the amount of blowing. Increases in the total normal force coefficient were observed and the increment in rolling moment was shown to be significant and almost linearly dependent on the jet blowing strength above 35 degrees angle of attack.

Flow mapping surveys illustrated the strong influence the co-flowing blowing configuration exerted upon the trajectory of the feeding sheet and consequently the vortex position. At low angles of attack, the cross-flow around the wing could be made to remain attached over the entire surface, recovering the attached flow solution. Favorable increments in wing drag may be expected due to the reorginisation of the flowfield.

Counter-flowing blowing was shown to exert little influence upon the normal force except for an isolated case at 20 degrees angle of attack and very low blowing. Although this was an isolated occurrence, the effect was considerable and if the mechanism could be identified, it may be further exploited over a wider range of conditions.

REFERENCES

1. Herbst, W.B. 'Dynamics of Air Combat', Journal of Aircraft Vol 20 No 7 pp594-598.

2. Orlik-Ruckemann, K.J. 'Aerodynamic Aspects of Aircraft Dynamics at High Angles of Attack' Journal of Aircraft Vol 20 No 9 pp737-752

3. Rao, D.M. 'Leading-Edge Vortex FLap Experiments on a 74-Deg. Delta Wing' NASA CR 159161, 1979

4. Marchman, J.F., Manor, D. and Plentovich, E.B. 'Performance Improvement of Delta Wings at Subsonic SPeeds Due to Vortex Flaps' AIAA Paper 80-1802, Aug. 1980.

5. Anglin E.L. and Satran D. 'Effects of Spanwise BLowing on Two Fighter Airplane Configurations' Journal of Aircraft Vol 17 No 12 1980.

6. Wood N.J. and Nielsen J. 'Circulation Control Airfoils - Past, Present and Future' AIAA Paper 85-0204 1985.

7. Lee J.C. and Wood N.J. 'Calibration and Data Reduction of a Five Hole Probe' JIAA TR-73.

TABLE 1

Delta Wing Pressure Tapping Locations

Row Number	1	2	3	4	5	6	7	8
X/C	0.182	0.273	0.364	0.455	0.546	0.636	0.727	0.909
Y/B		Tappings common to both upper and lower surfaces						
0.0833						*	*	*
0.1667	*	*	*	*	*	*	*	*
0.2500		*	*	*	*	*	*	*
0.3333	*	*	*	*	*	*	*	*
0.4167		*	*	*	*	*	*	*
0.5000	*	*	*	*	*	*	*	*
0.5833		*	*	*	*	*	*	*
0.6667	*	*	*	*	*	*	*	*
0.7500		*	*	*	*	*	*	*
0.8333	*	*	*	*	*	*	*	*
		Tappings around leading edge, * = under wall jet + = on both surfaces						
0.8839								+
0.9086		*	*	*	*	*	*	
0.9210								+
0.9366		*	*	*	*	*	*	
0.9534								+
0.9610		*	*	*	*	*	*	
0.9785								+
0.9798		*	*	*	*	*	*	
0.9917		*	*	*	*	*	*	
0.9945								+
0.9958		*	*	*	*	*	*	
1.0000								*

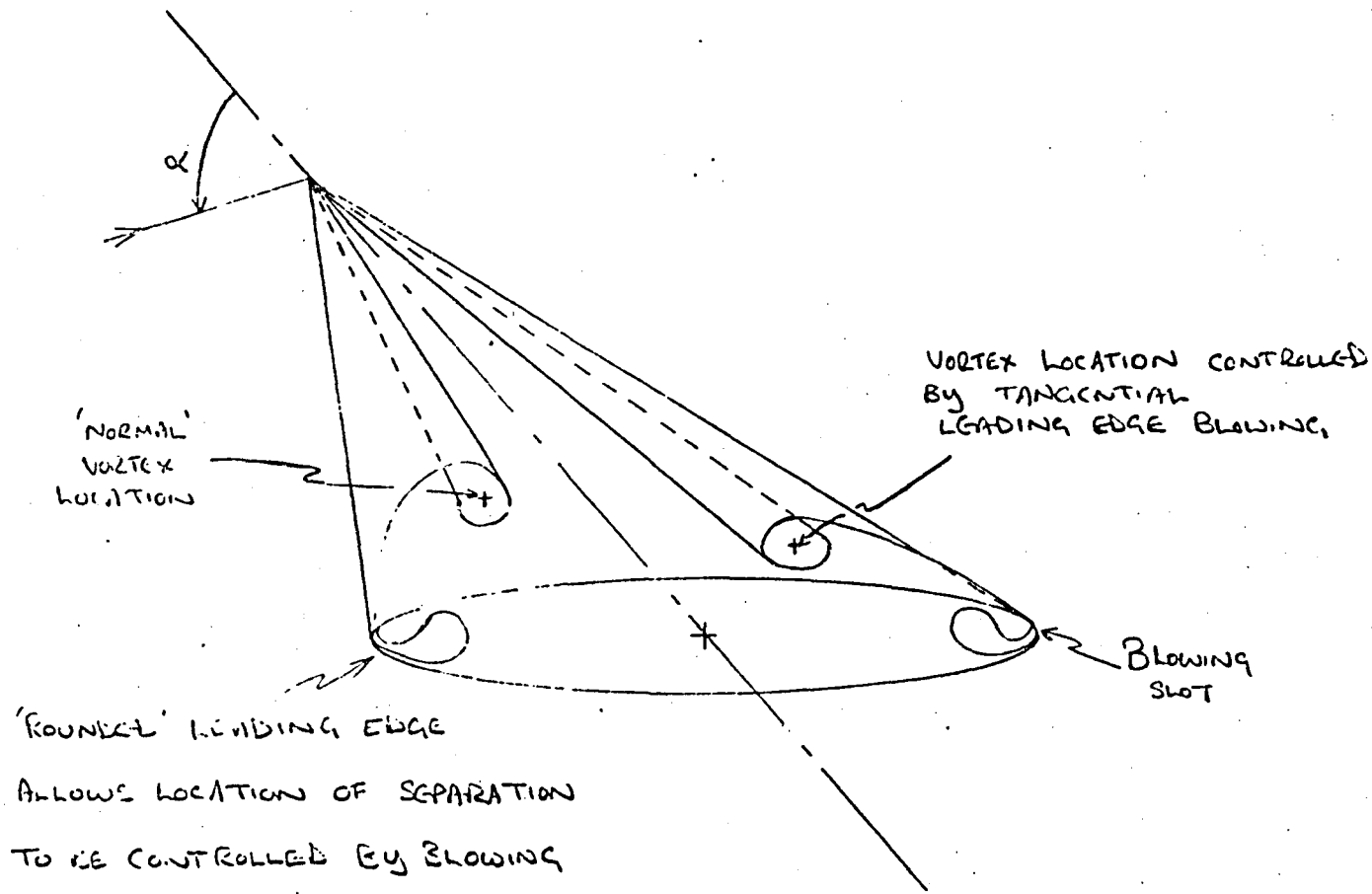

FIGURE 1: SCHEMATIC OF FLOWFIELD

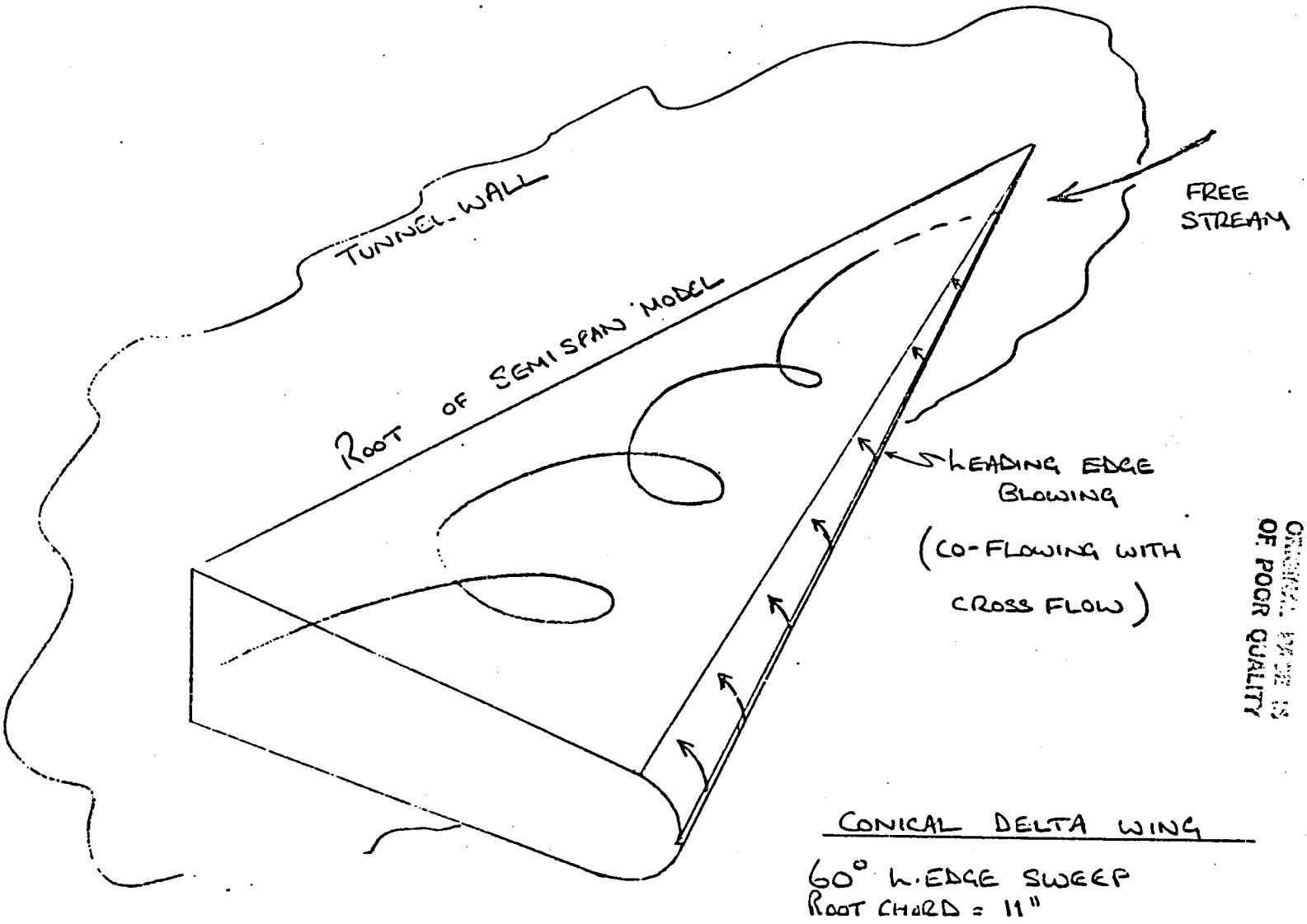

FIGURE 2: SIMPLIFIED VIEW OF WIND TUNNEL MODEL

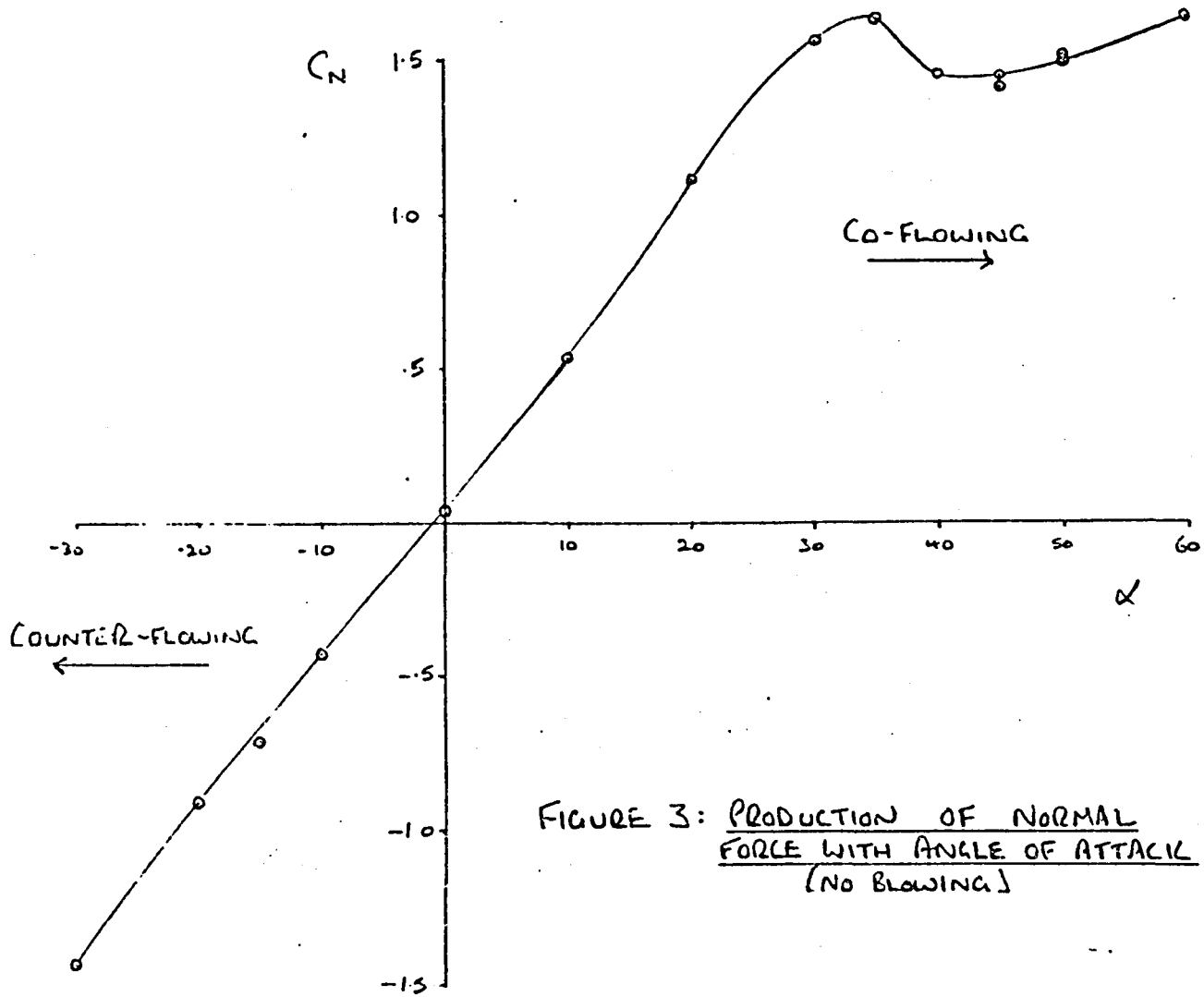

FIGURE 3: PRODUCTION OF NORMAL FORCE WITH ANGLE OF ATTACK (NO BLOWING)

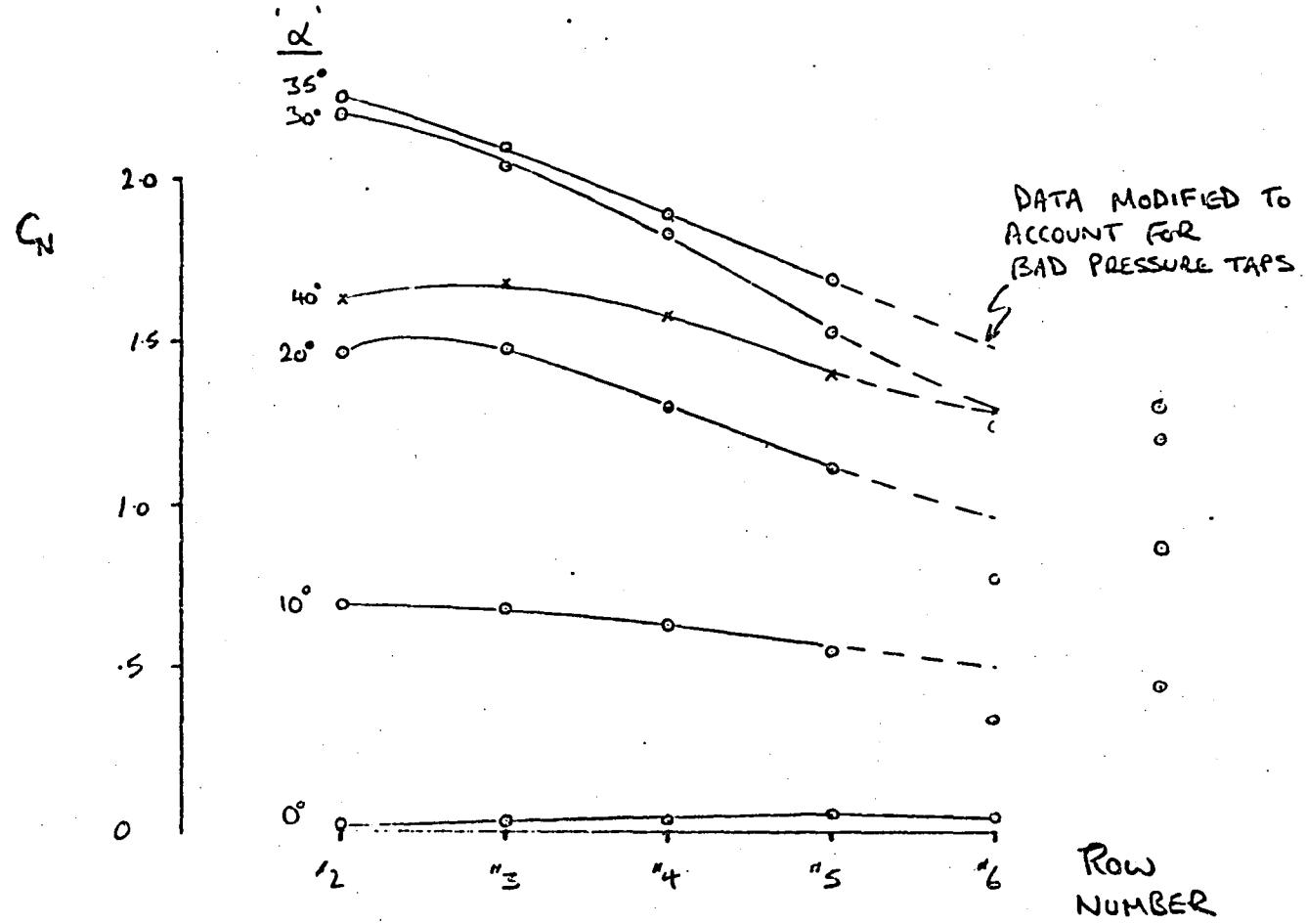

FIGURE 4: UNBLOWN LONGITUDINAL LOAD DISTRIBUTIONS (CO-FLOWING)

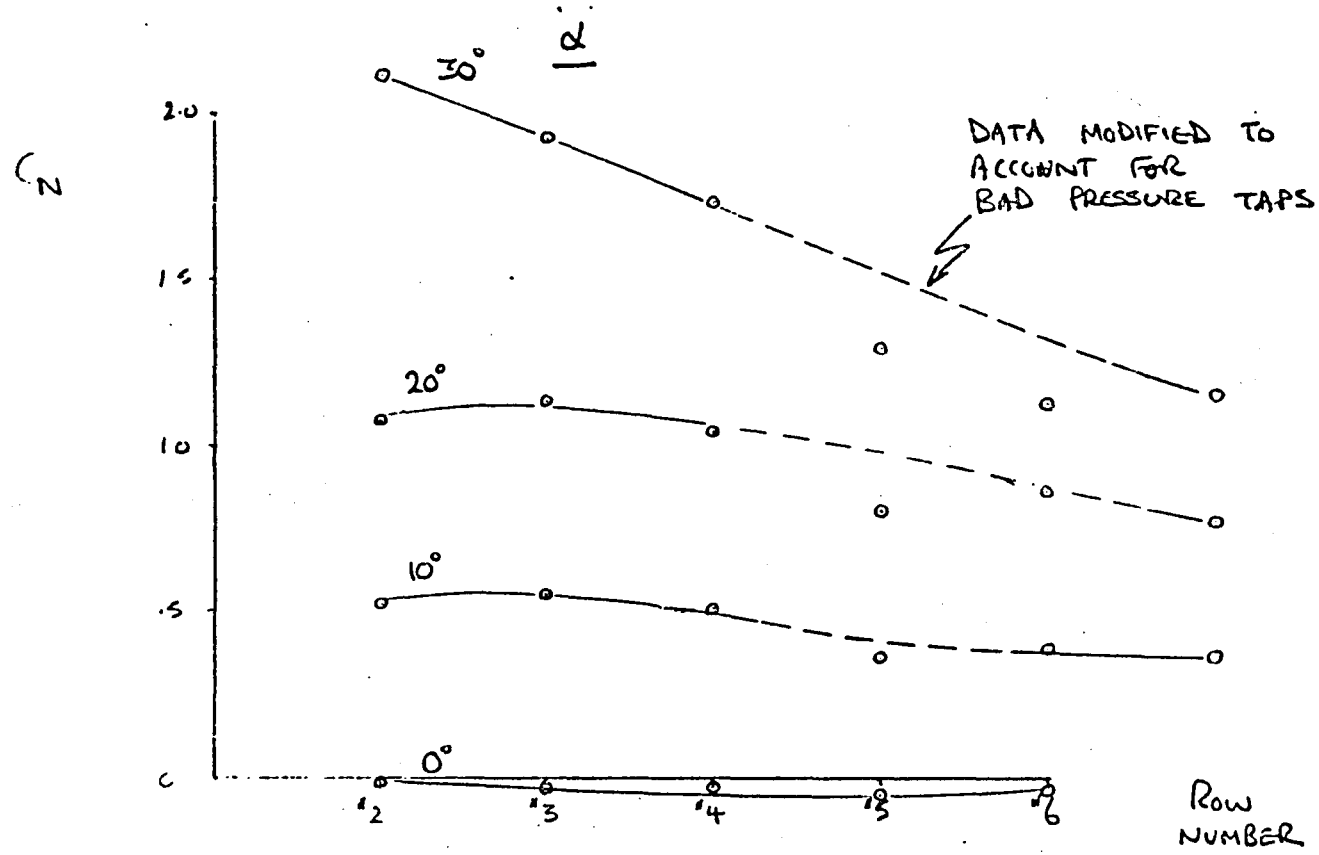

FIGURE 5: UNBLOWN LONGITUDINAL LOAD DISTRIBUTIONS (COUNTER-FLOWING)

No Blowing (#2)

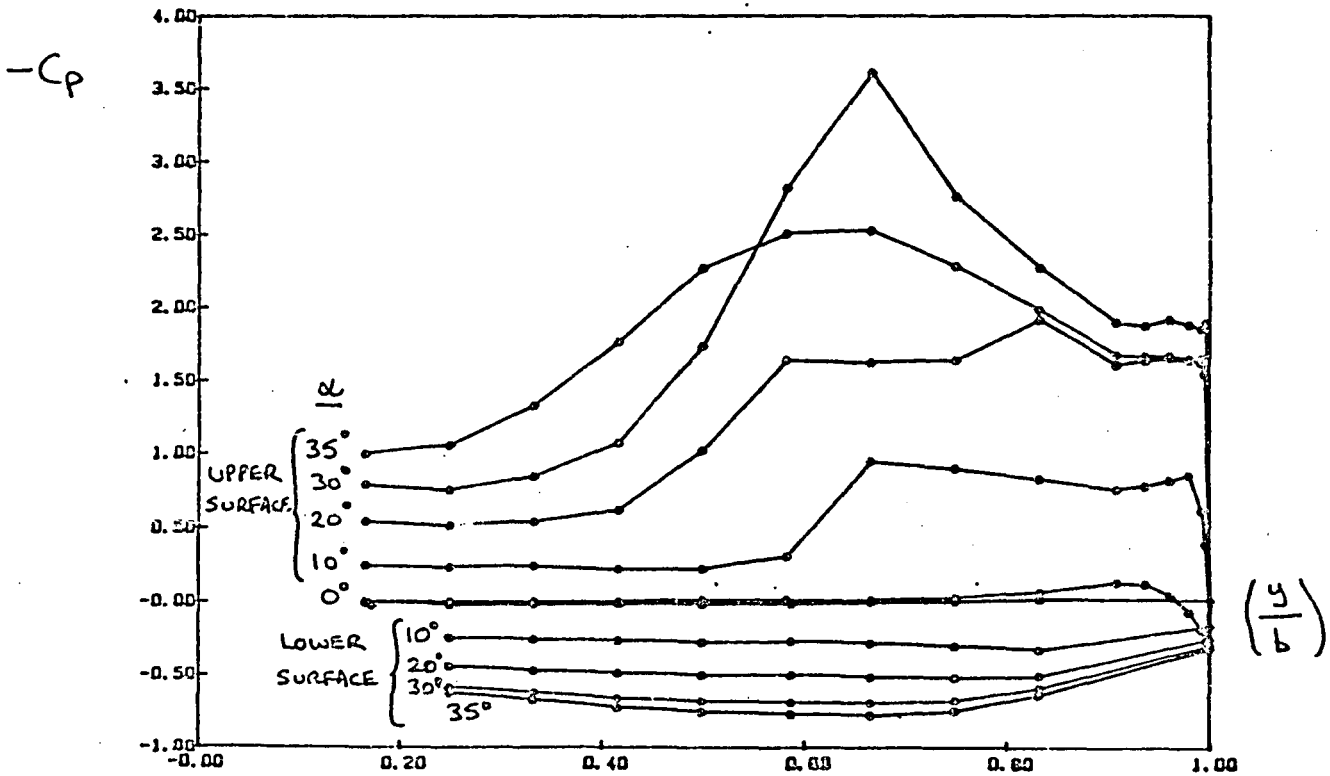

FIGURE 6: UNBLOWN PRESSURE DISTRIBUTIONS - ROW 2

No Blowing (#3)

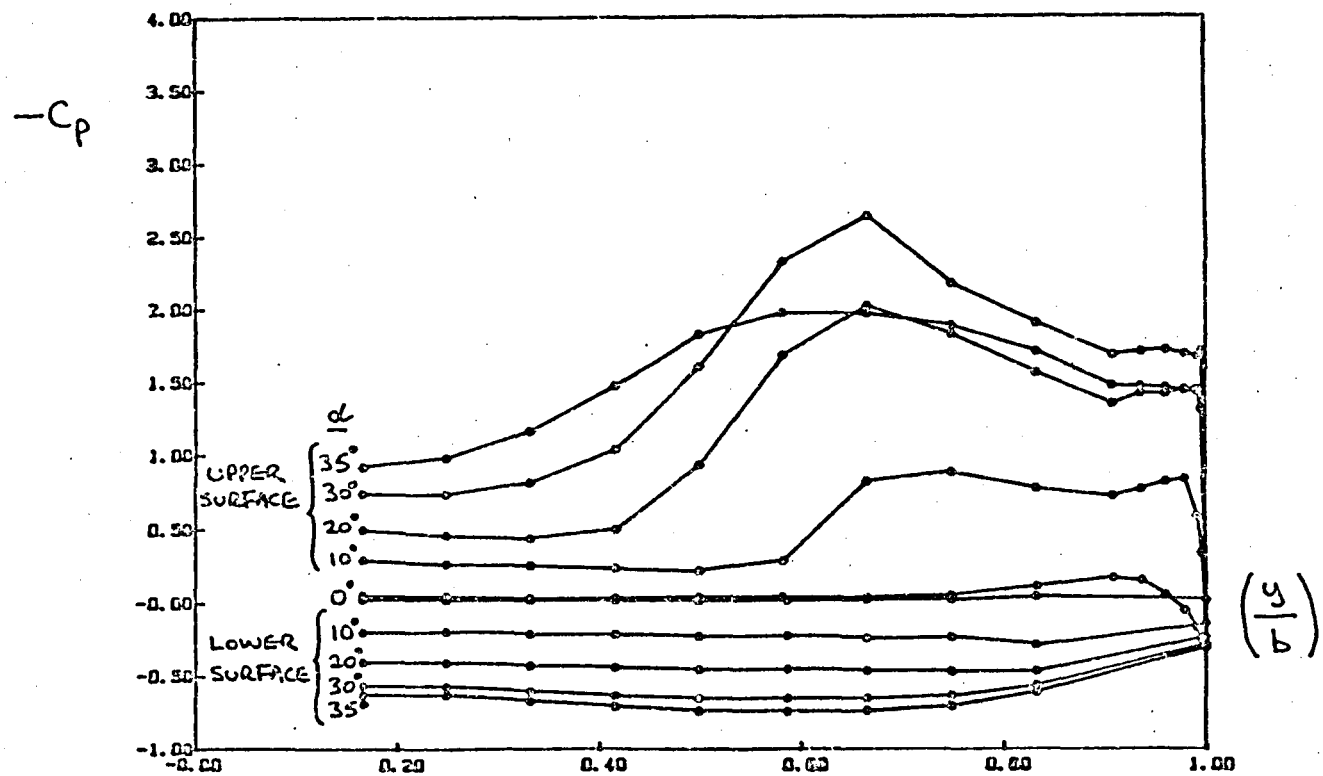

FIGURE 7: UNBLOWN PRESSURE DISTRIBUTIONS - ROW 3

No Blowing (#4)

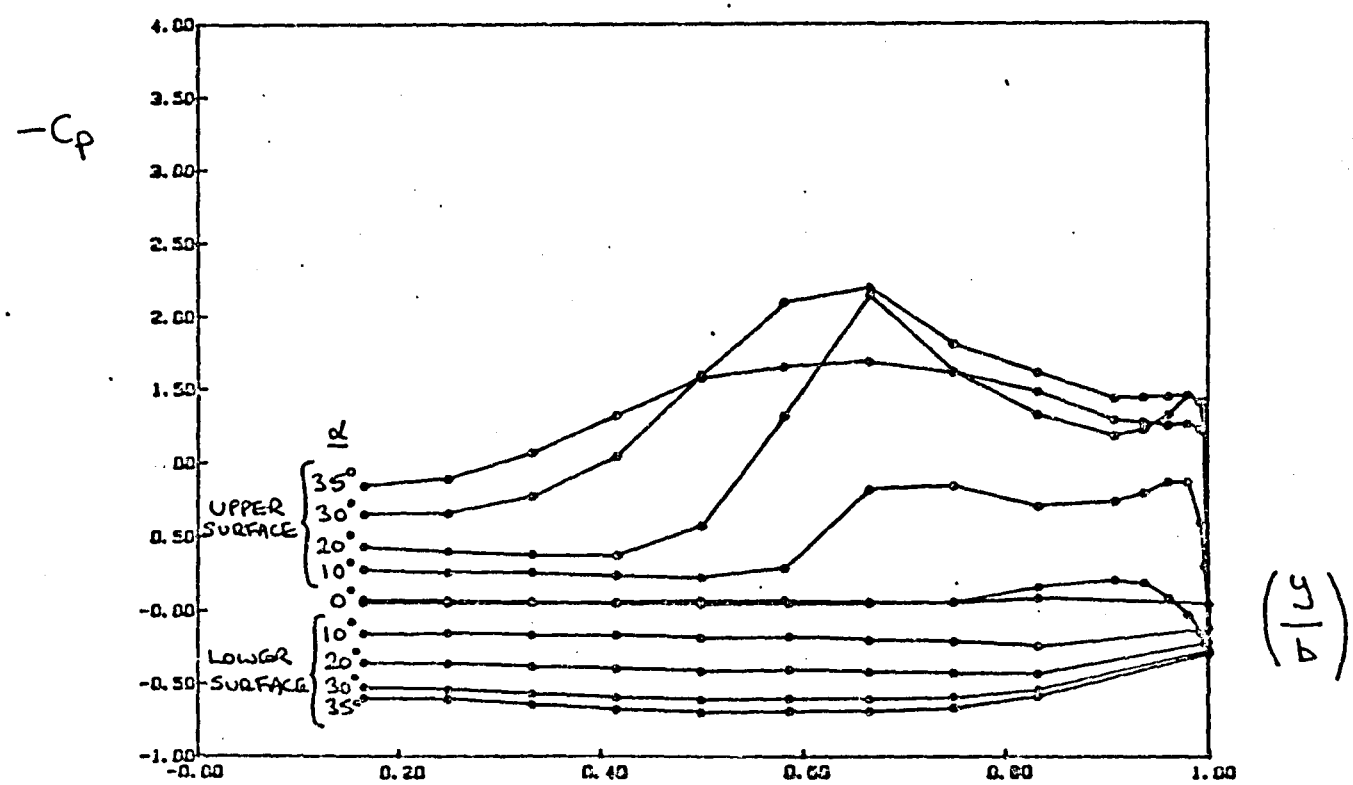

FIGURE 8: UNBLOWN PRESSURE DISTRIBUTIONS - ROW 4

No Blowing (#5)

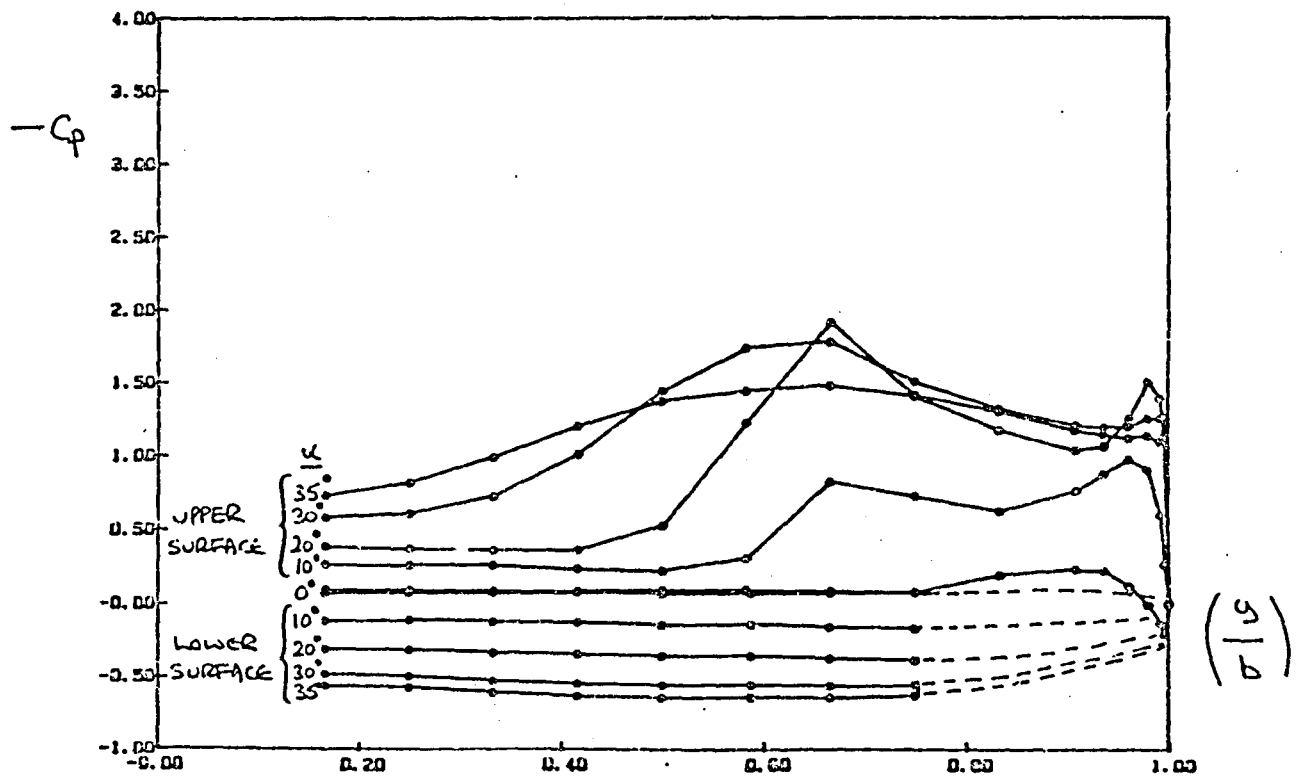

FIGURE 9: UNBLOWN PRESSURE DISTRIBUTIONS - ROW 5

No Blowing (#6)

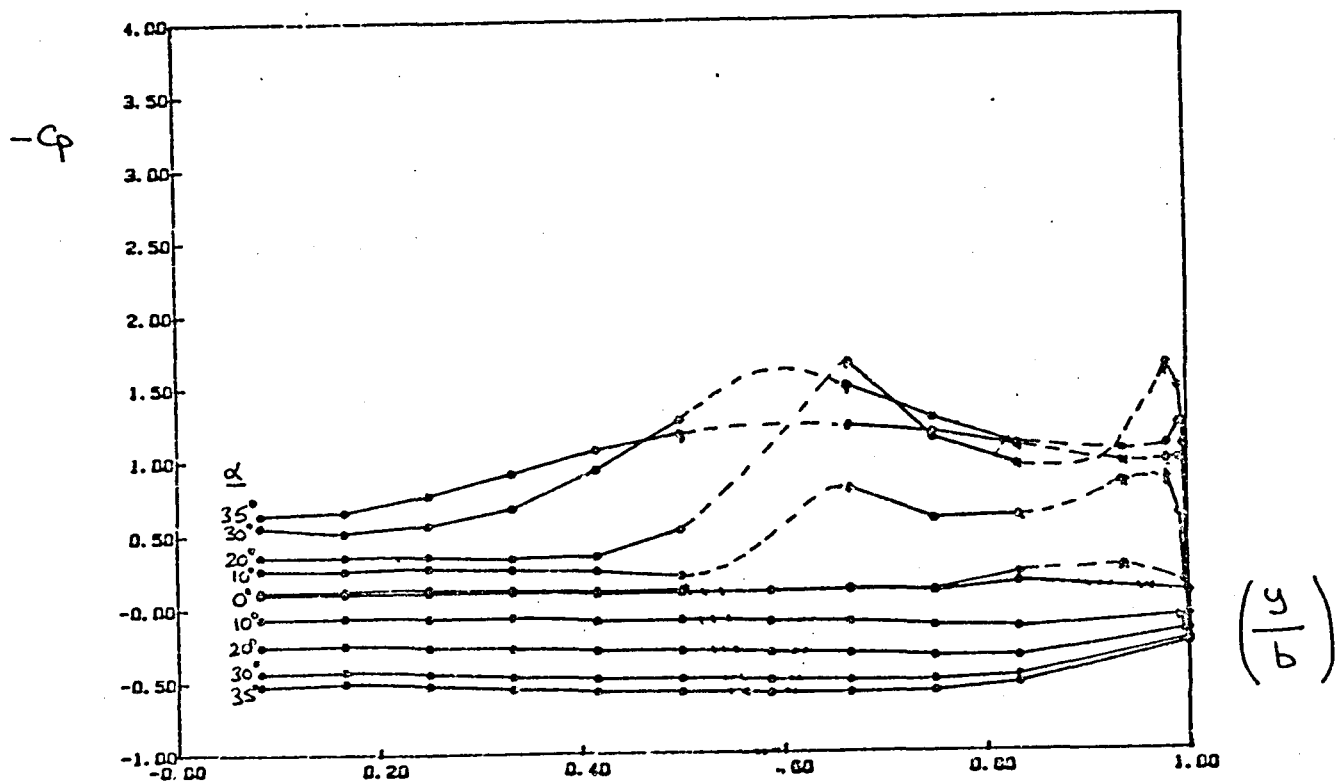

FIGURE 10: UNBLOWN PRESSURE DISTRIBUTIONS - ROW 6

No Blowing (#8)

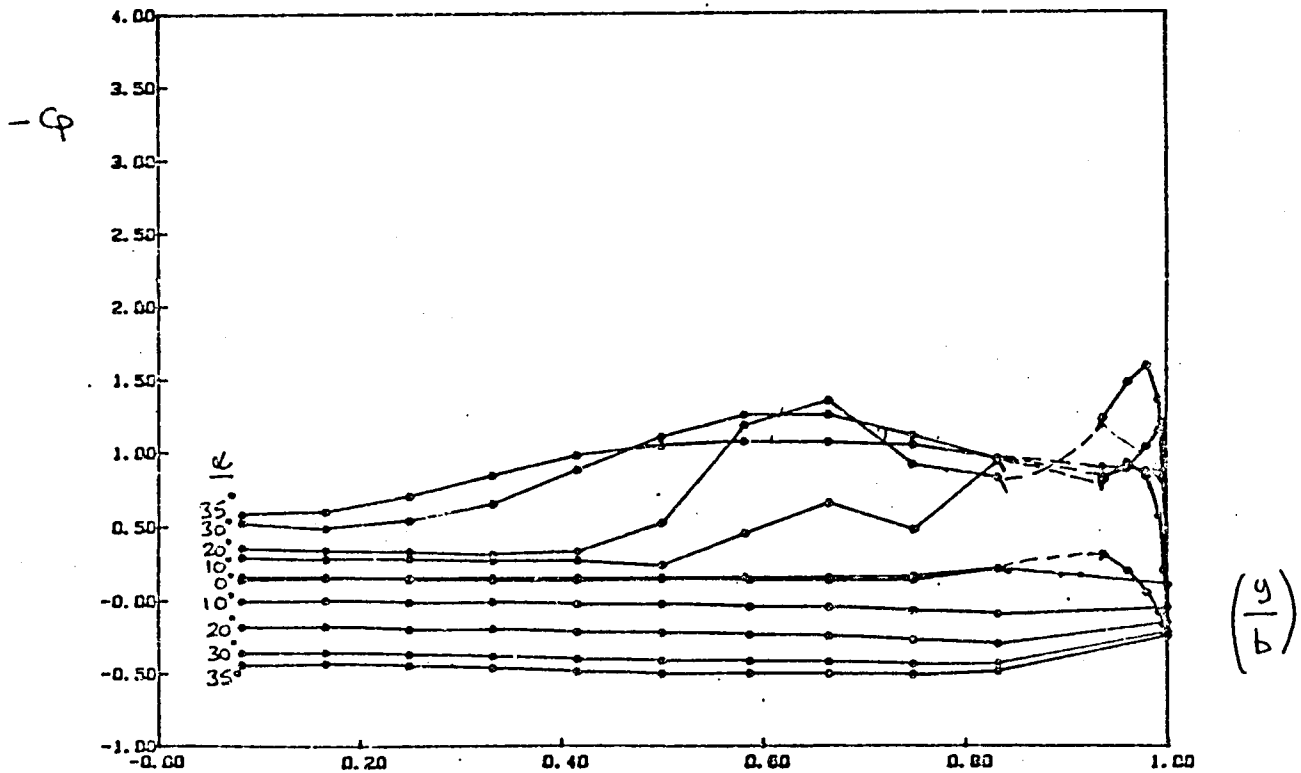

FIGURE 11: UNBLOWN PRESSURE DISTRIBUTIONS - ROW 7

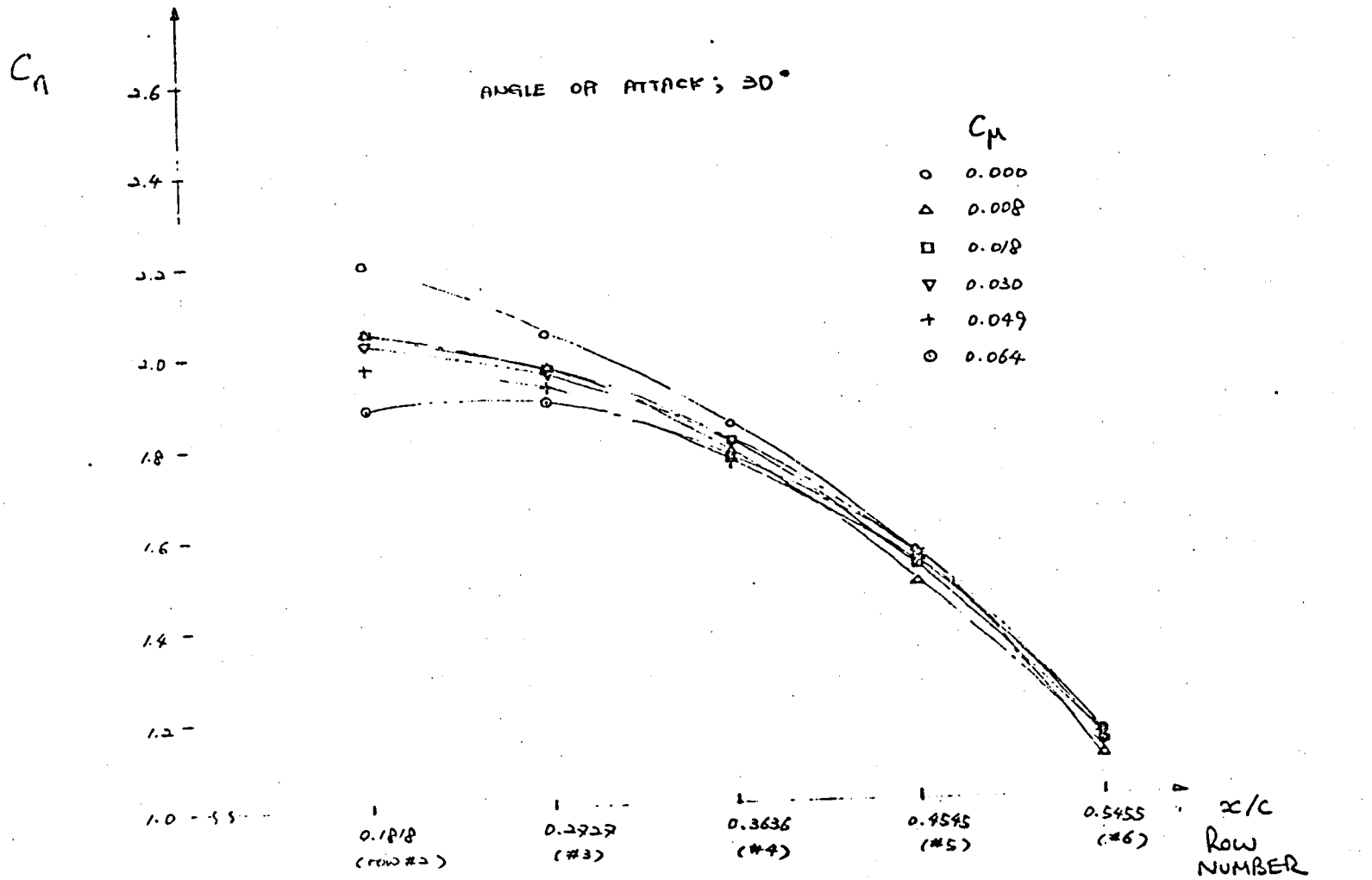

FIGURE 12a: LONGITUDINAL LOAD DISTRIBUTIONS, $\alpha = 30°$ CO-FLOWING CONFIGURATION

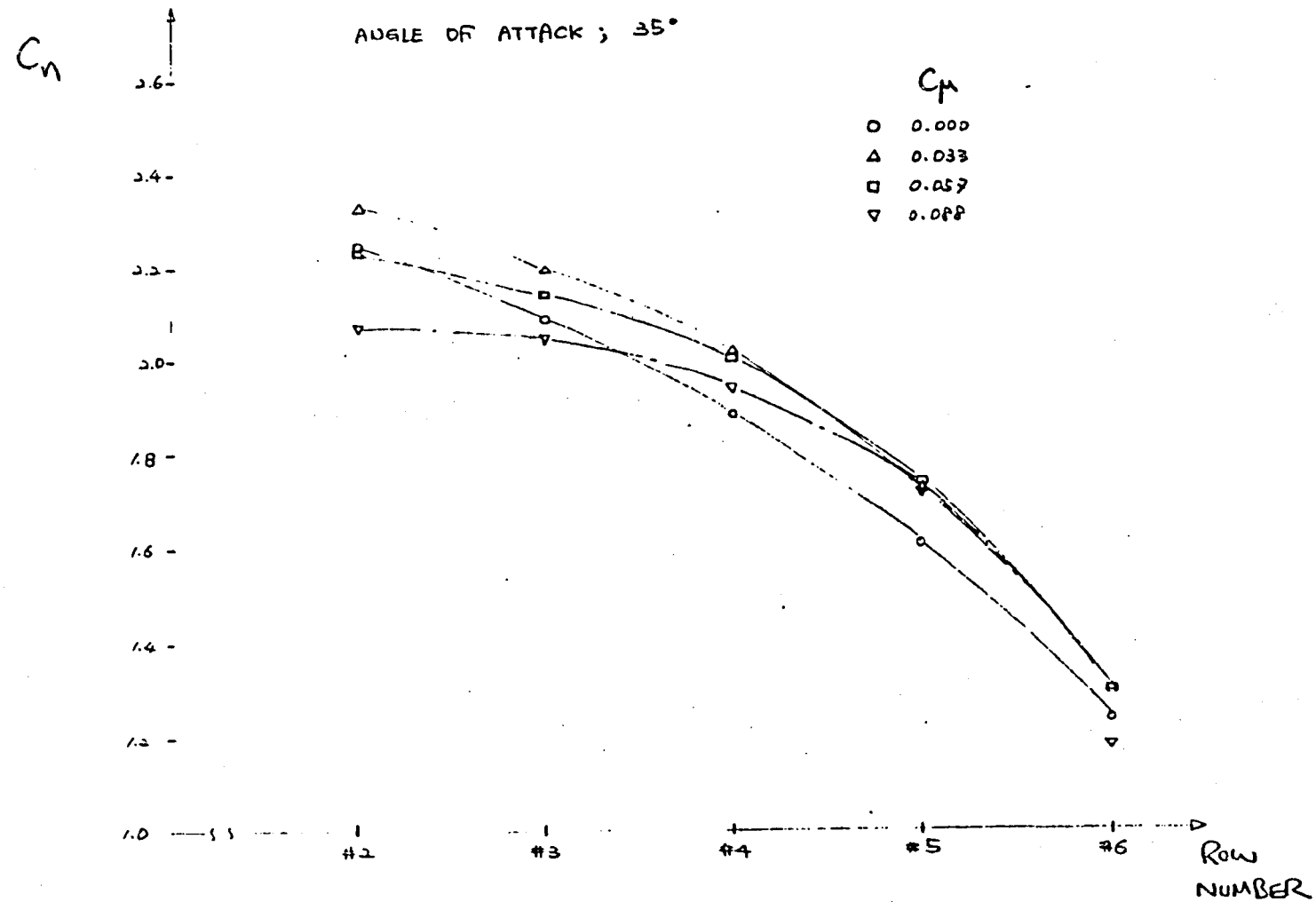

FIGURE 12 b: $\alpha = 35°$

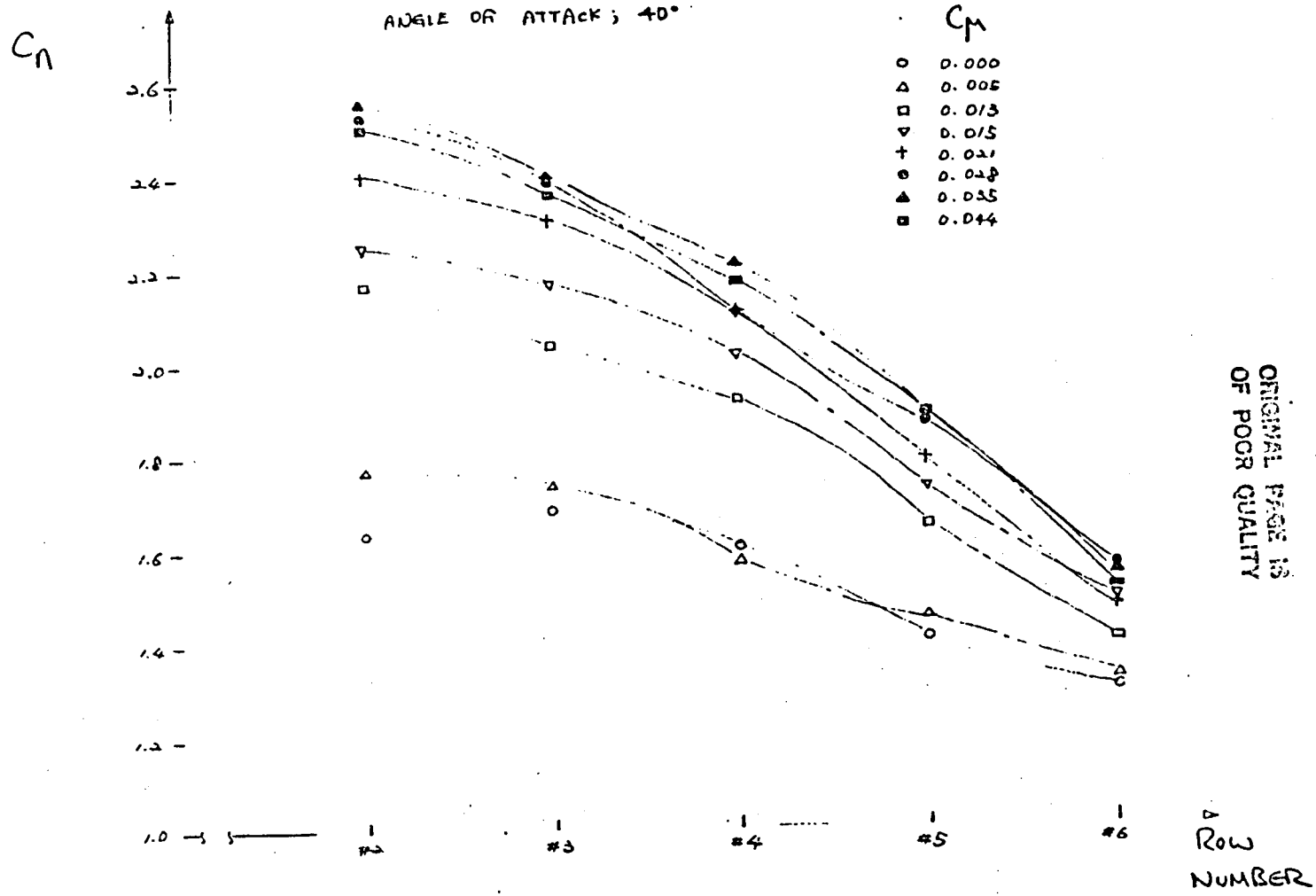

FIGURE 12c: $\alpha = 40°$

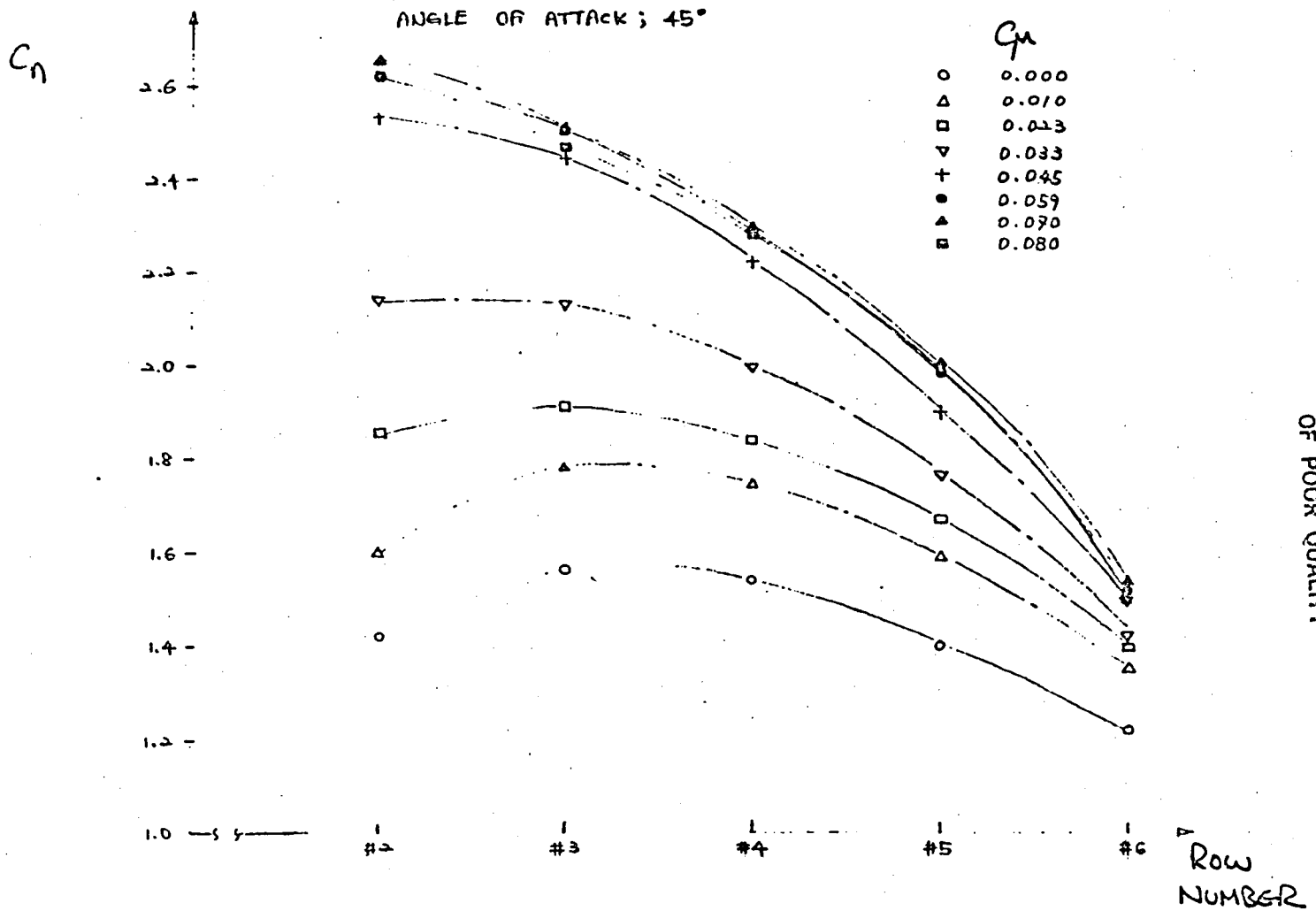

FIGURE 12 d: $\alpha = 45°$

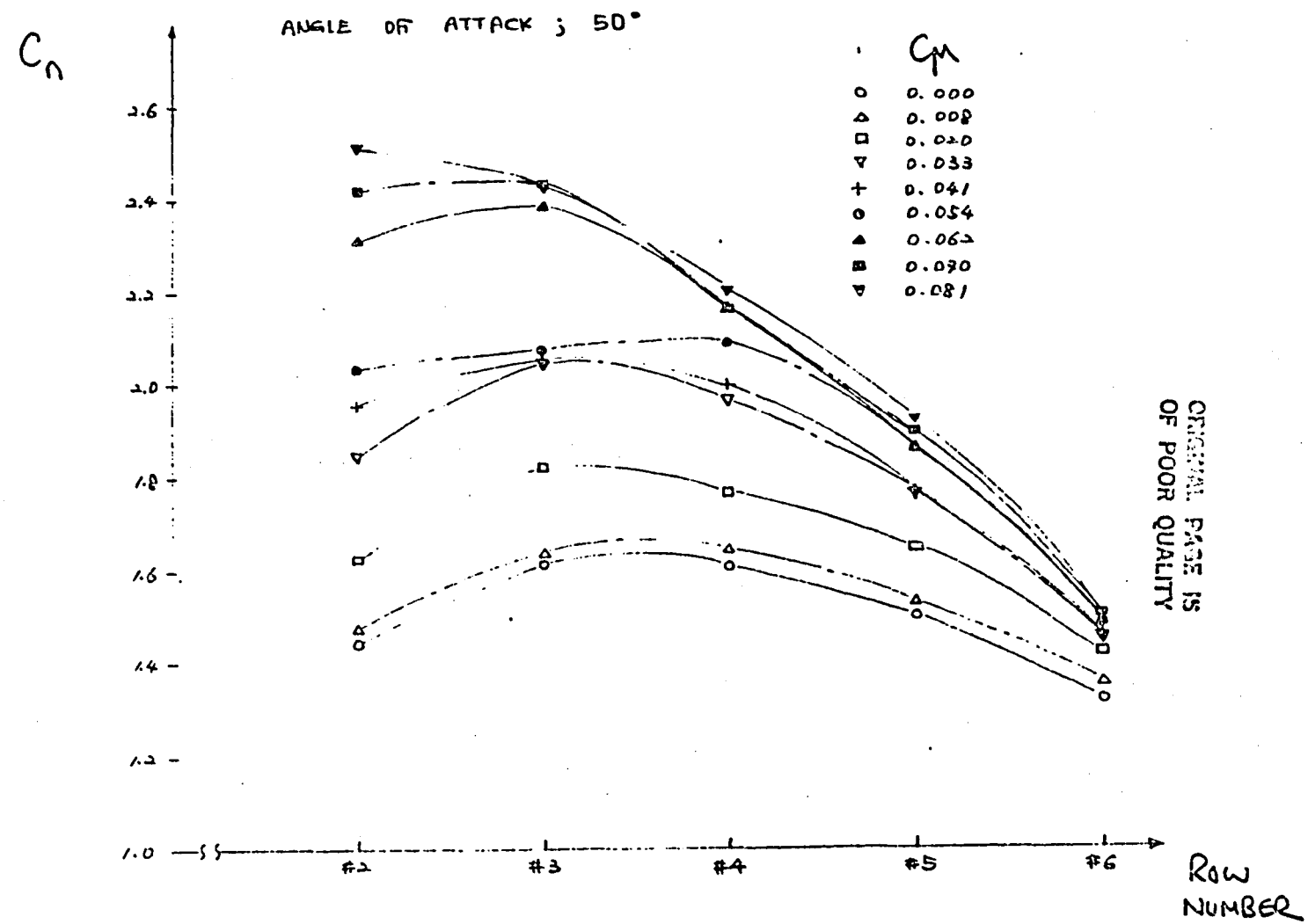

FIGURE 12e: $\alpha = 50°$

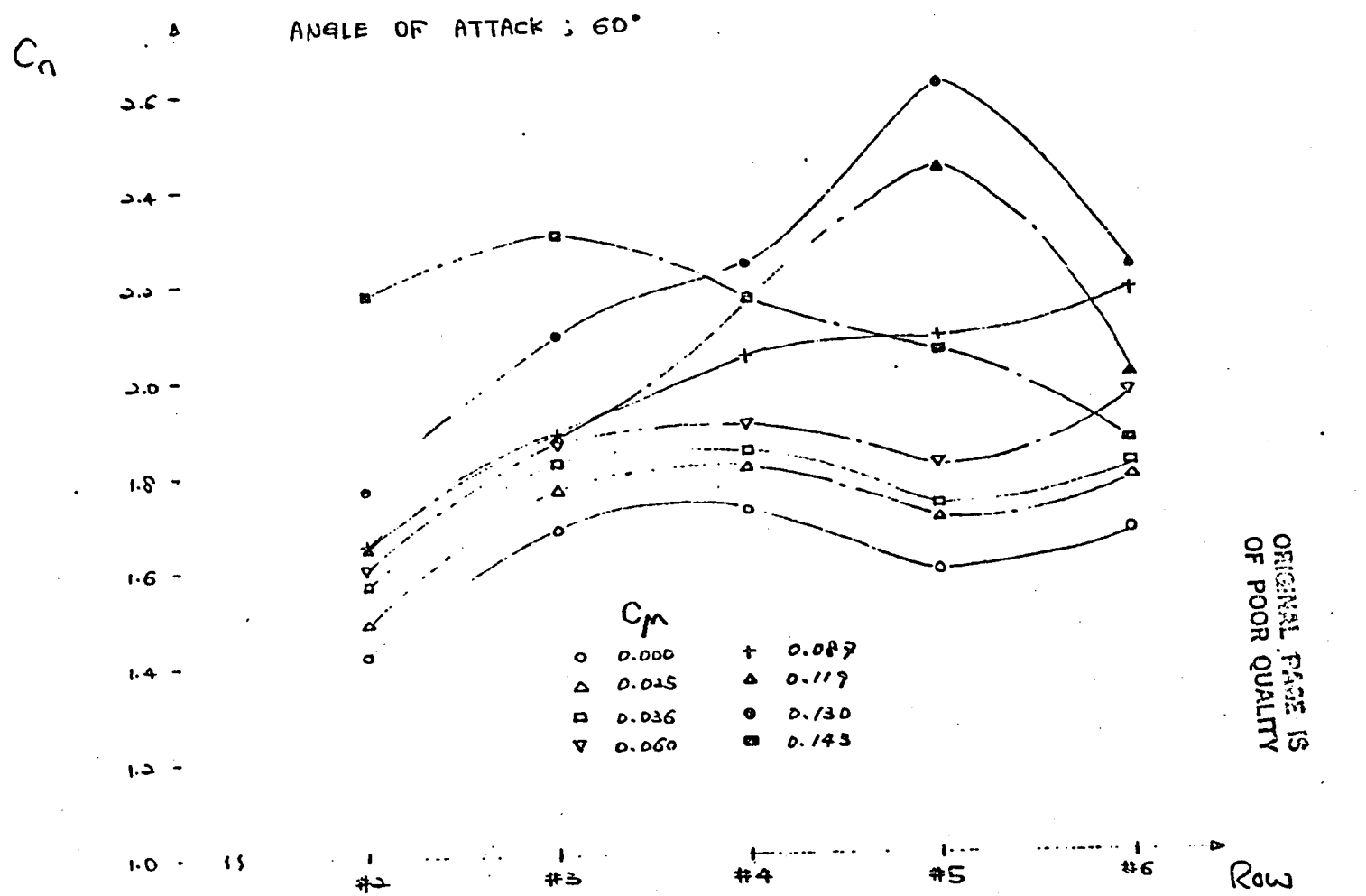

FIGURE 12f: $\alpha = 60°$

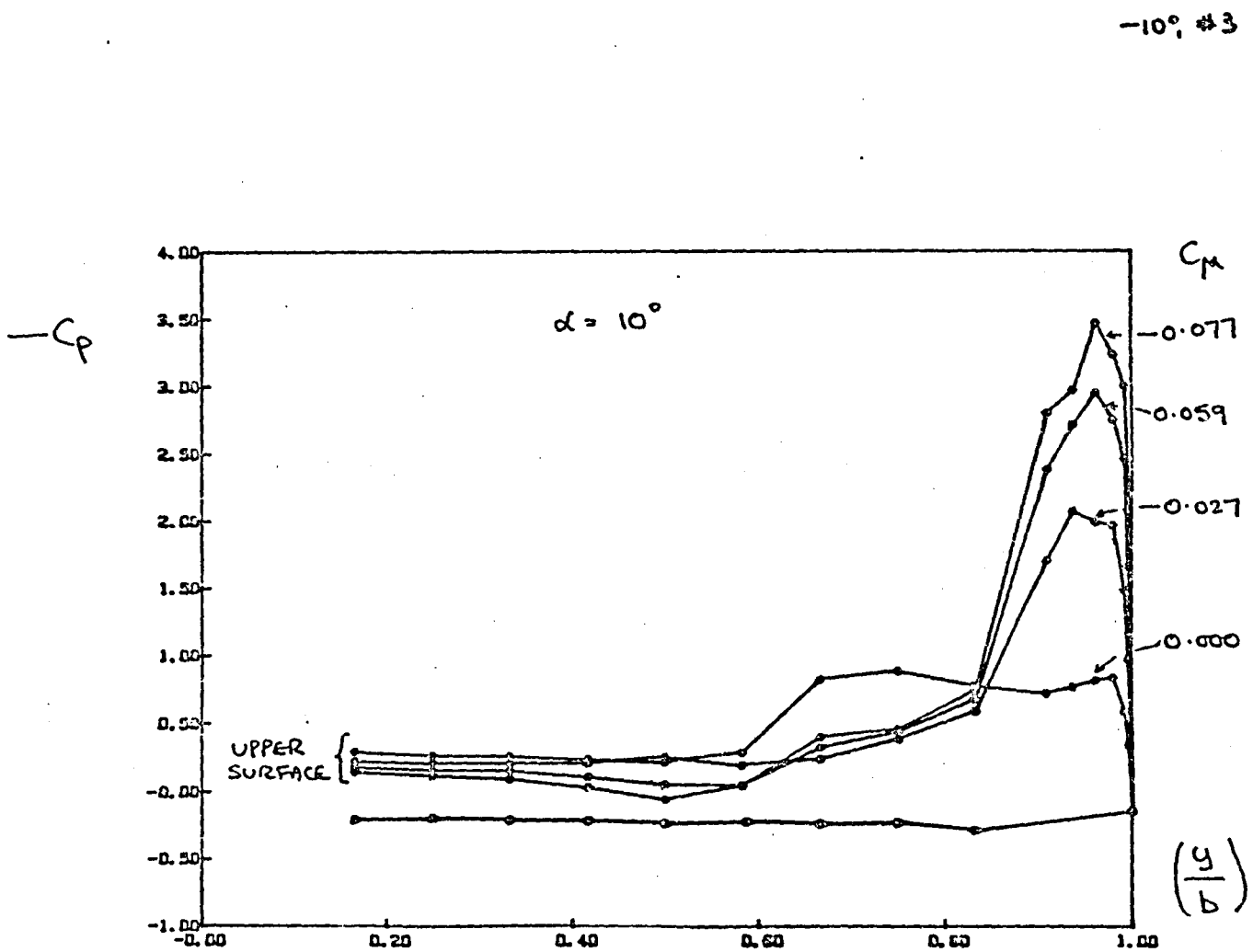

FIGURE 13a: PRESSURE DISTRIBUTION, ROW 3, CO-FLOWING CONFIGURATION

$\alpha = -10°$ (#4)

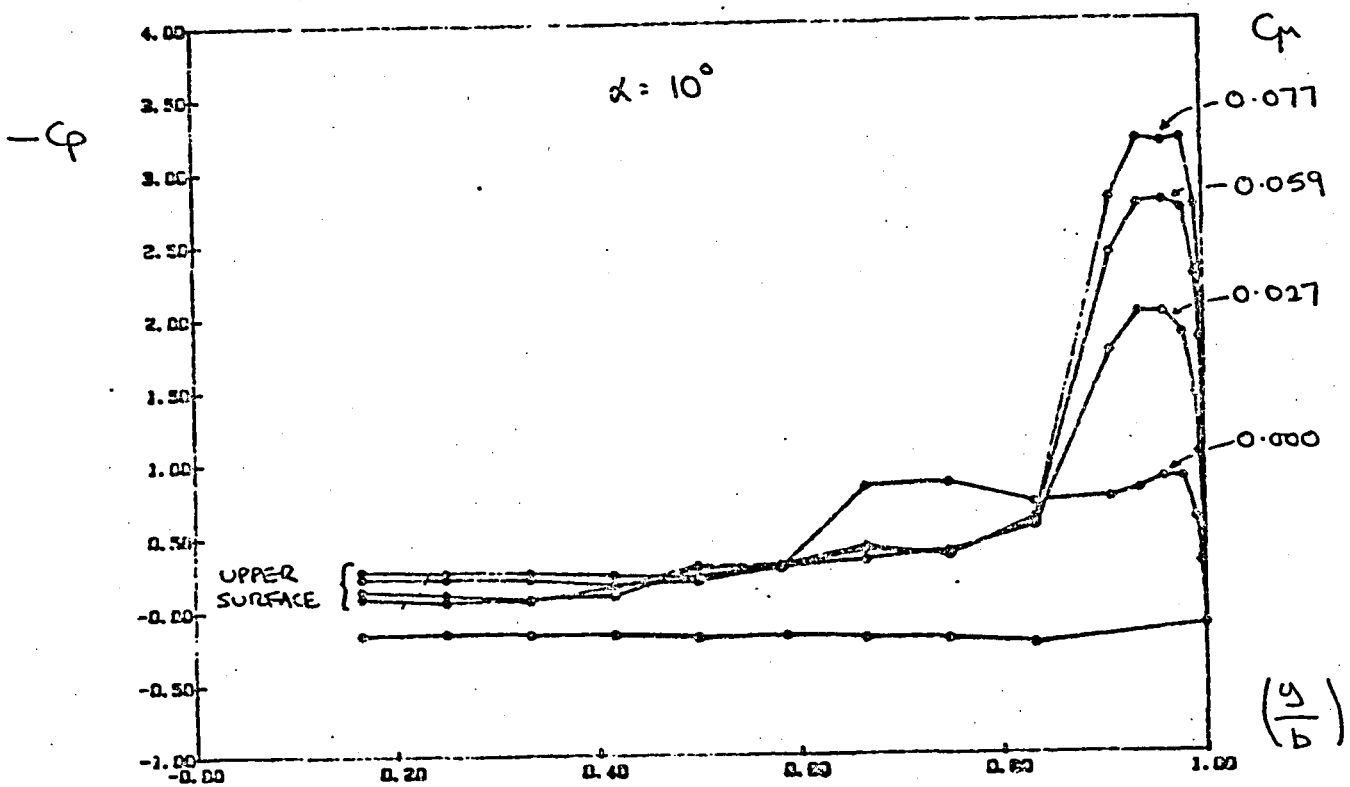

FIGURE 13 b: Row 4

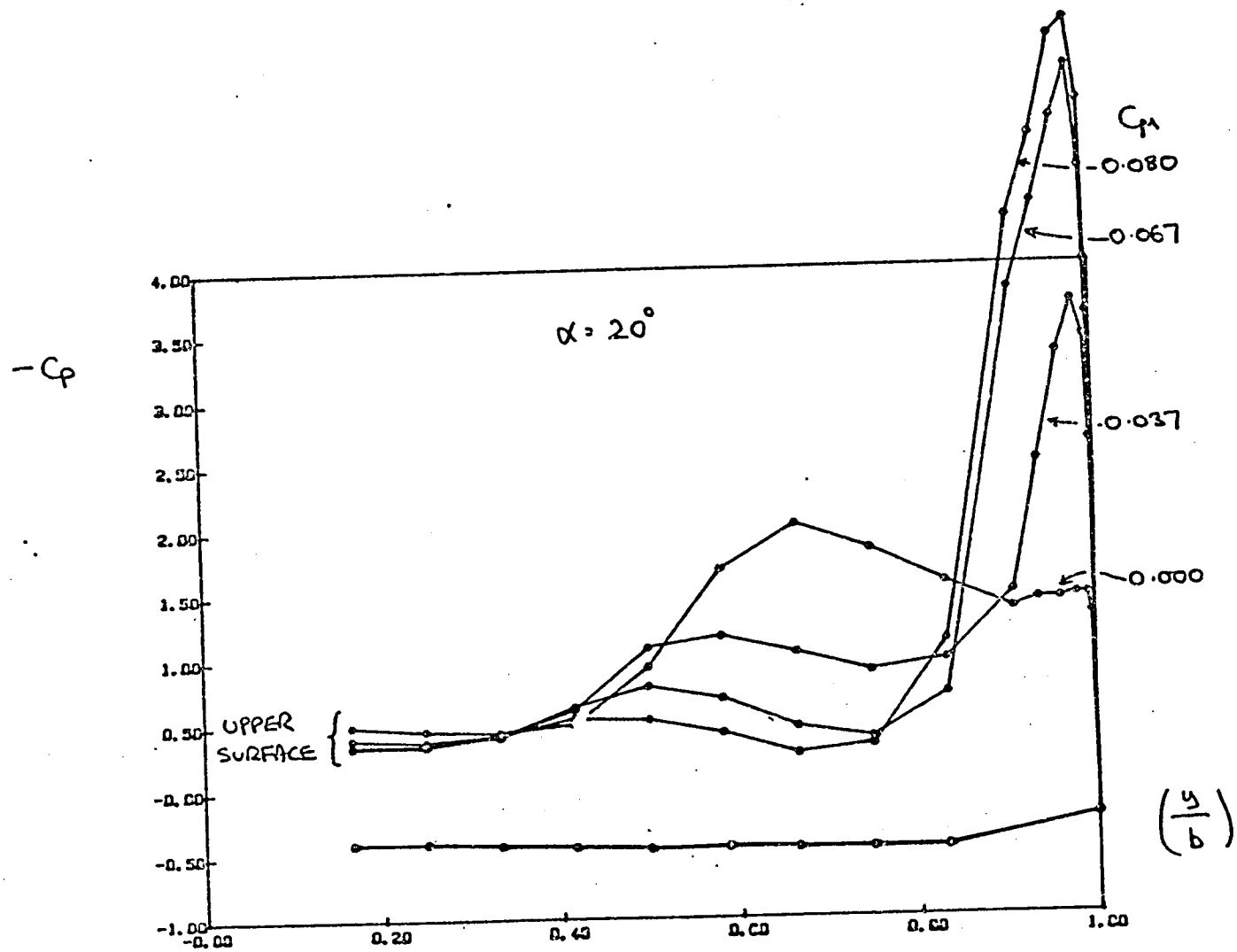

FIGURE 14a: PRESSURE DISTRIBUTION, ROW 3, CO-FLOWING CONFIGURATION

ANGLE −20° (#4)

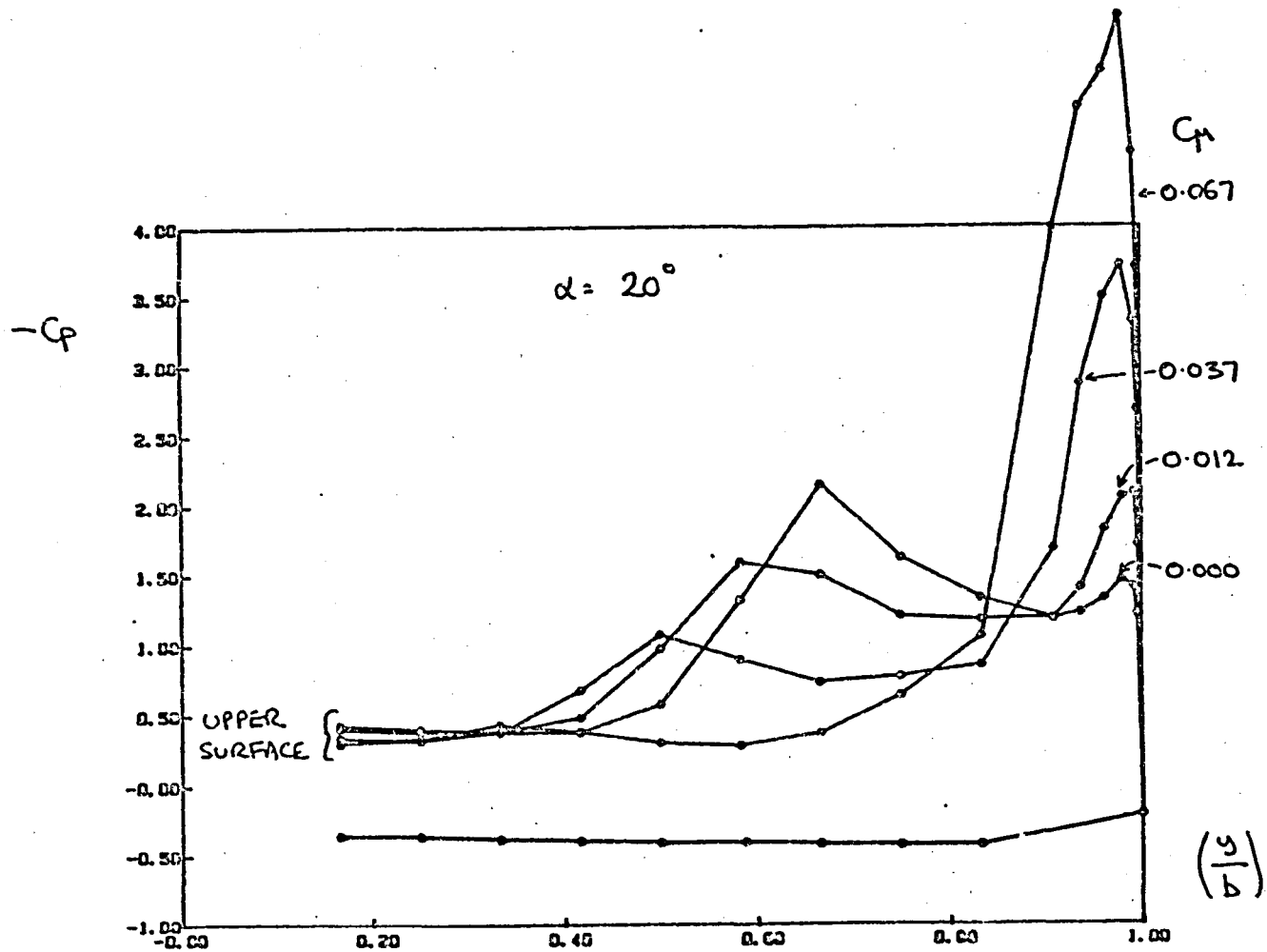

FIGURE 14b: Row 4

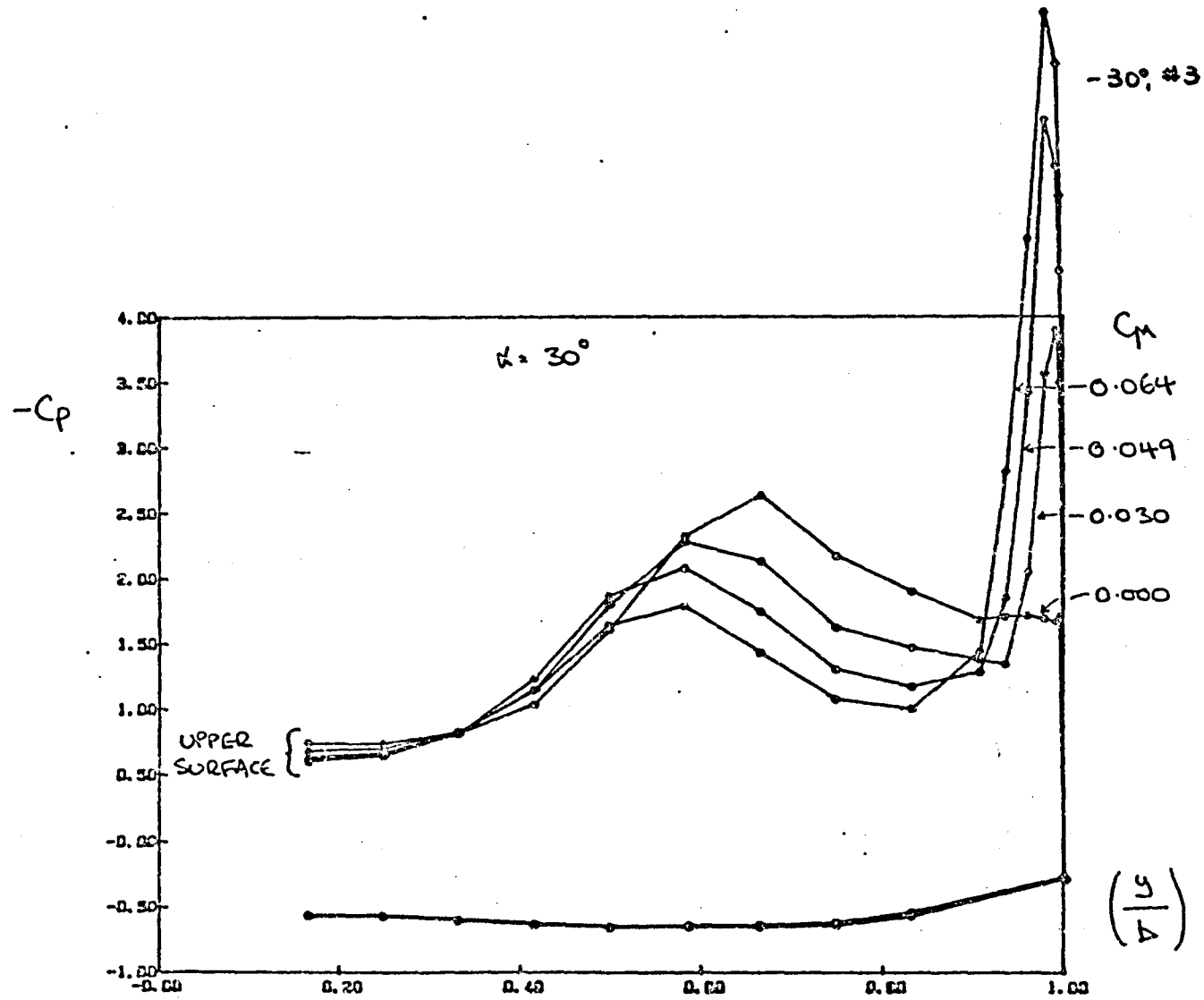

FIGURE 15a: PRESSURE DISTRIBUTIONS, ROW 3, CO-FLOWING CONFIGURATION

ANGLE -30° (#4)

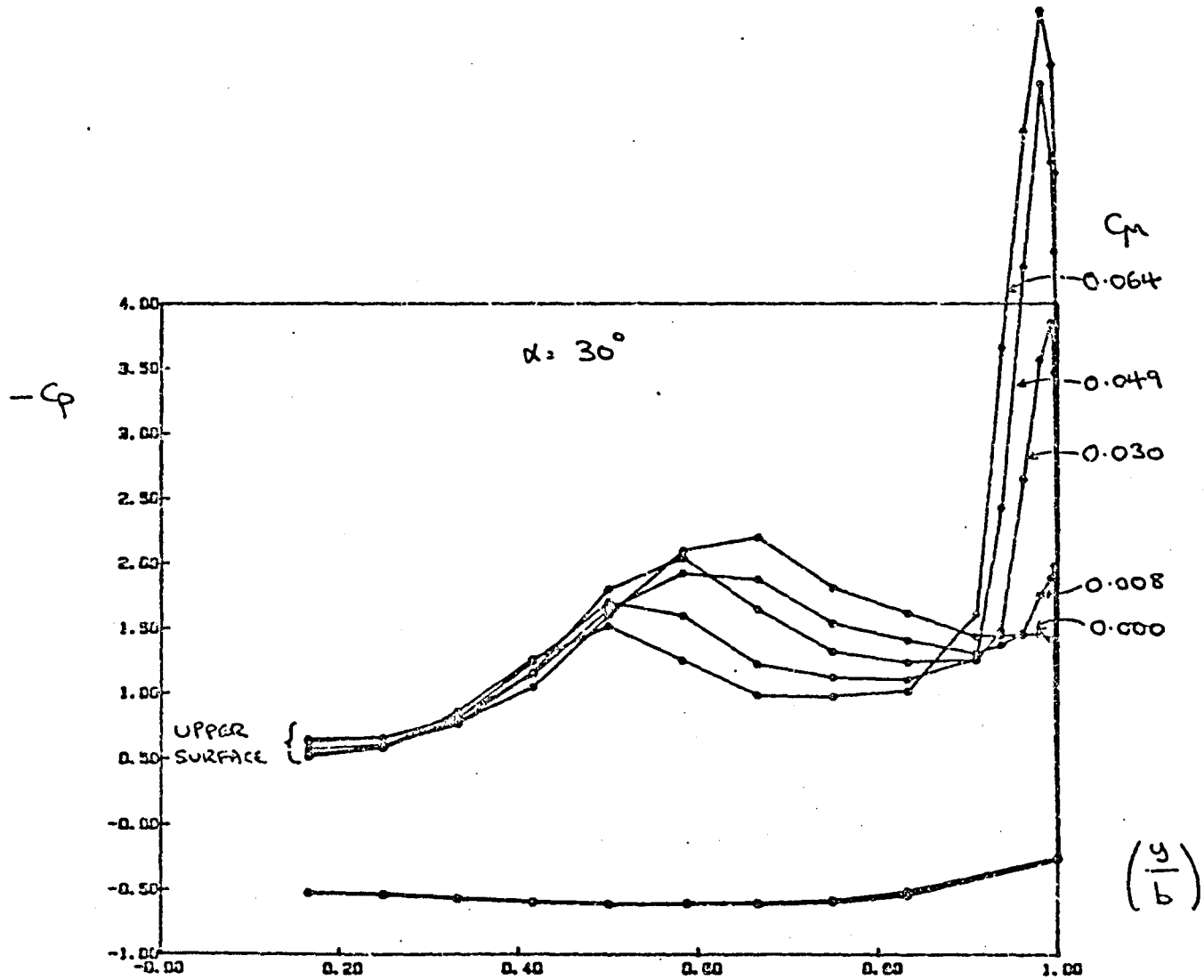

FIGURE 15b: Row 4

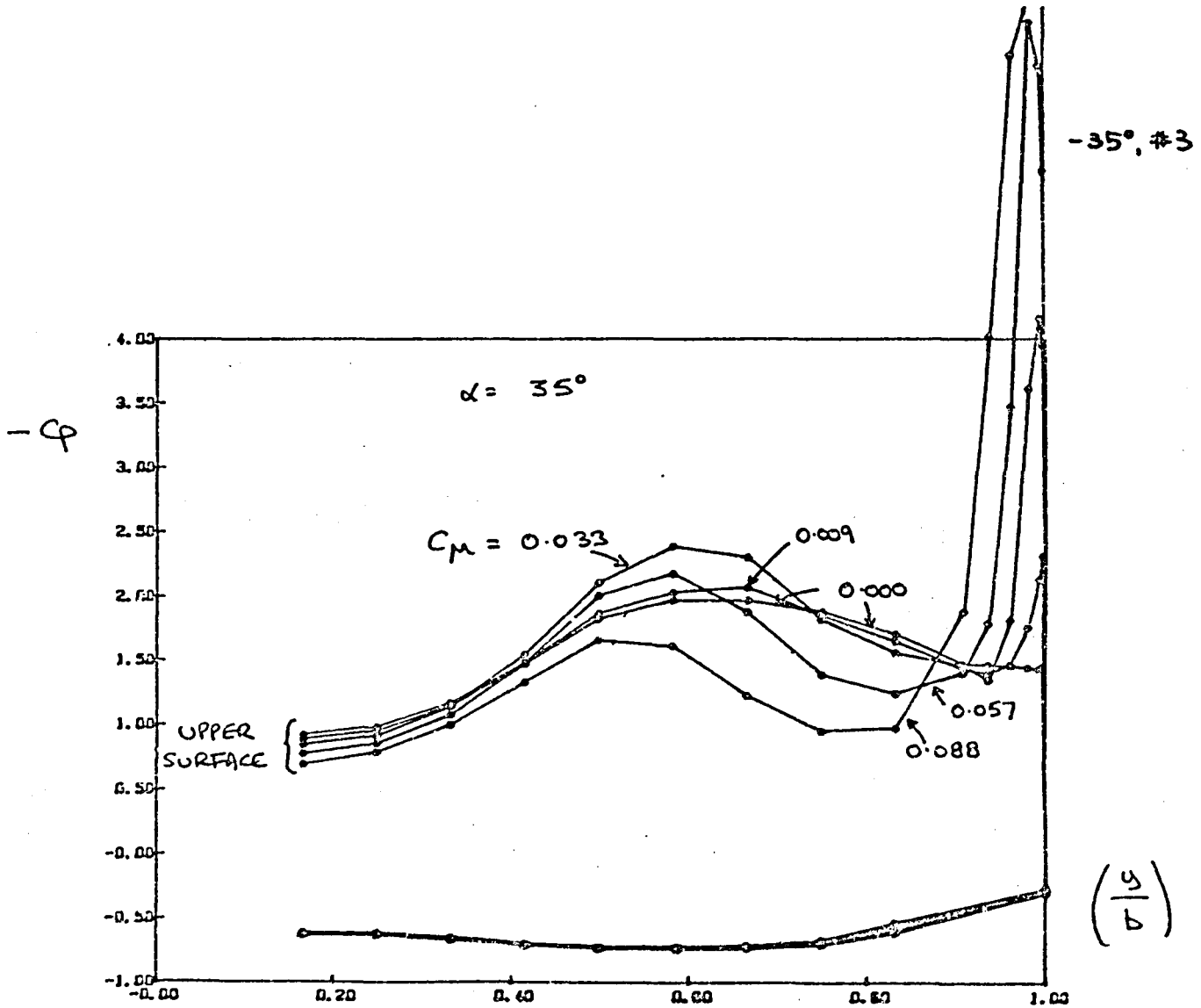

FIGURE 16a: PRESSURE DISTRIBUTIONS, ROW 3, CO-FLOWING CONFIGURATION

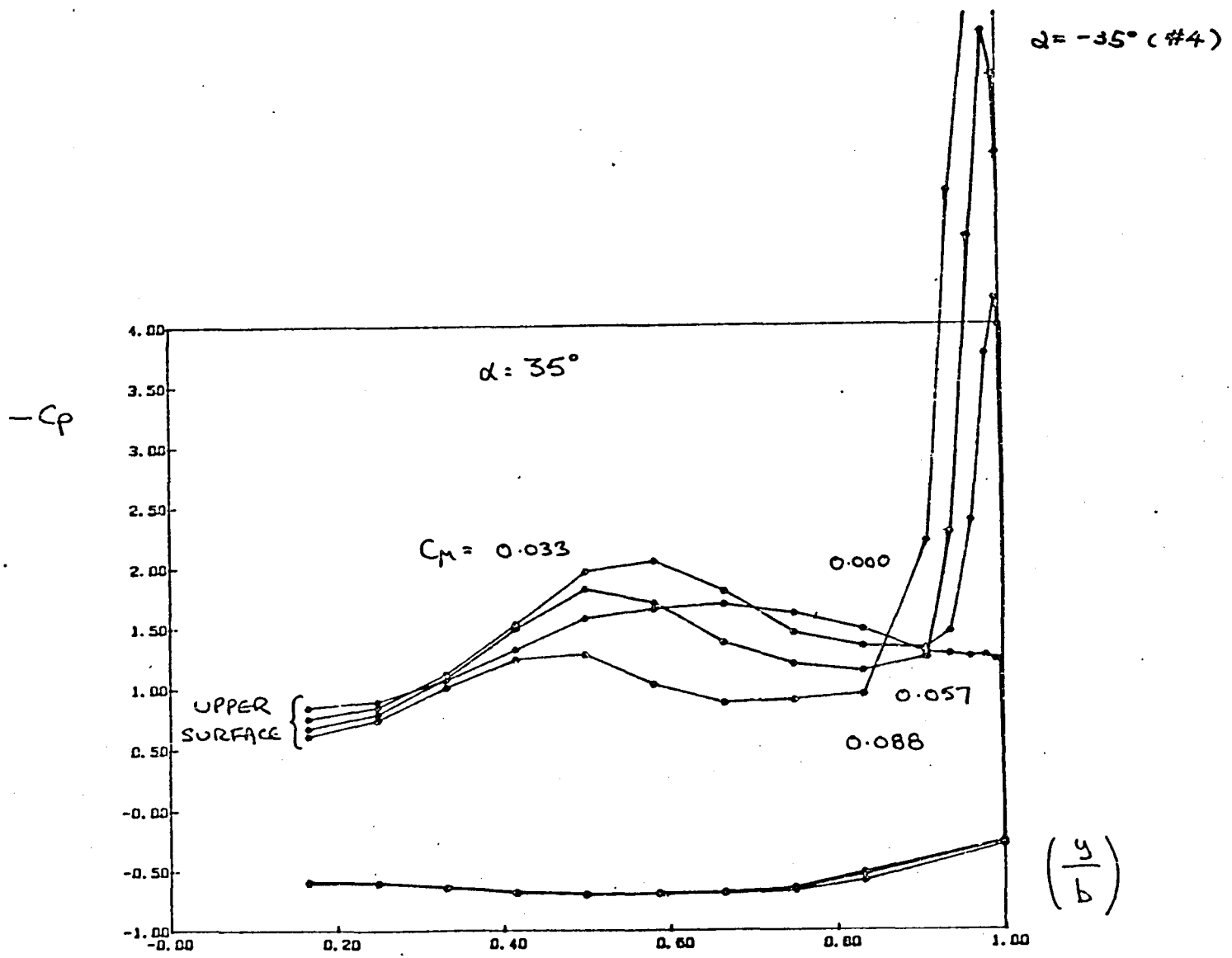

FIGURE 16 b: Row 4

-40°, #3

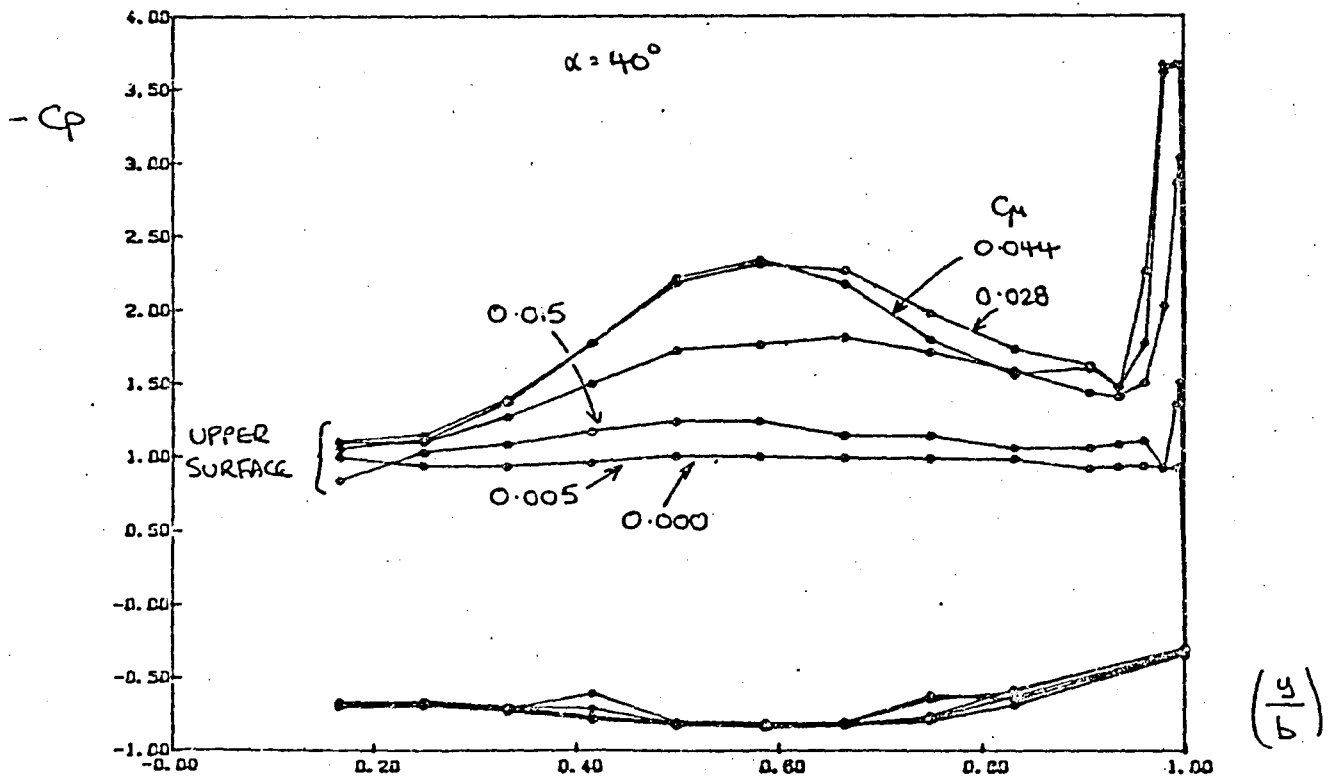

FIGURE 17a: PRESSURE DISTRIBUTIONS, ROW 3, CO-FLOWING CONFIGURATION

ANGLE -40° (#4)

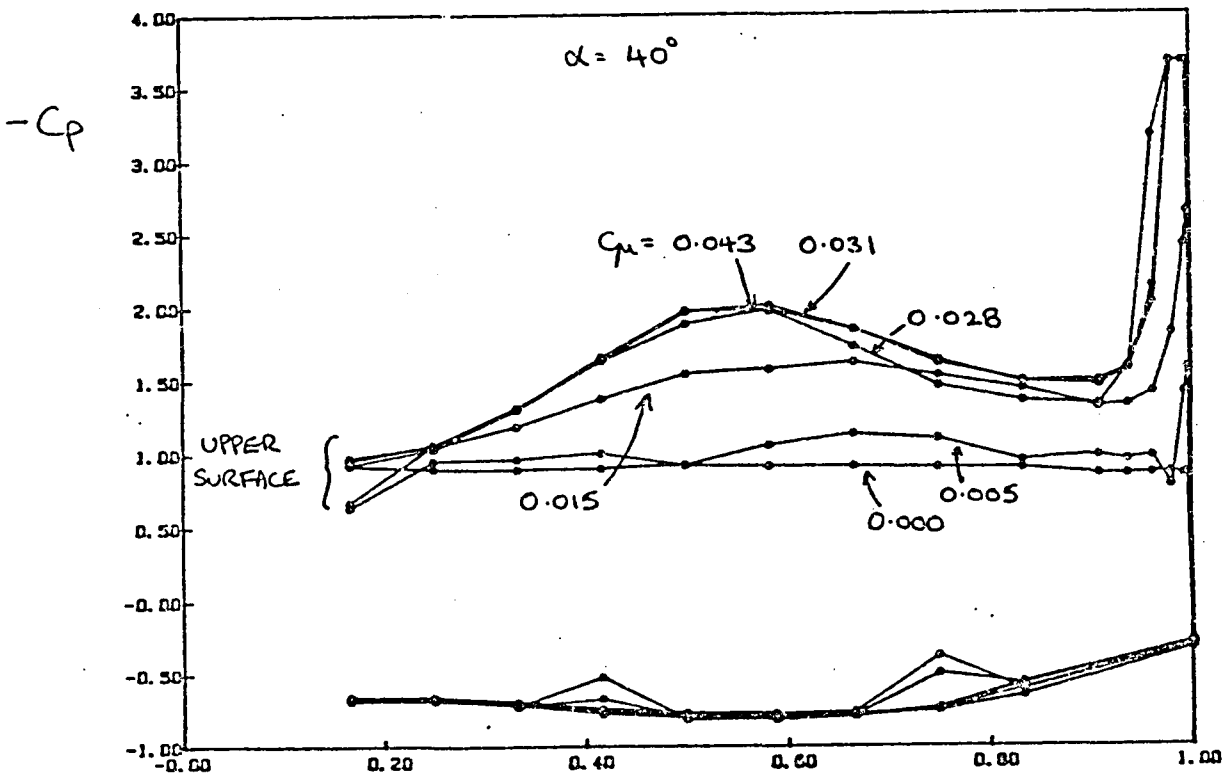

$-C_p$

$\left(\frac{y}{b}\right)$

FIGURE 17 b: ROW 4

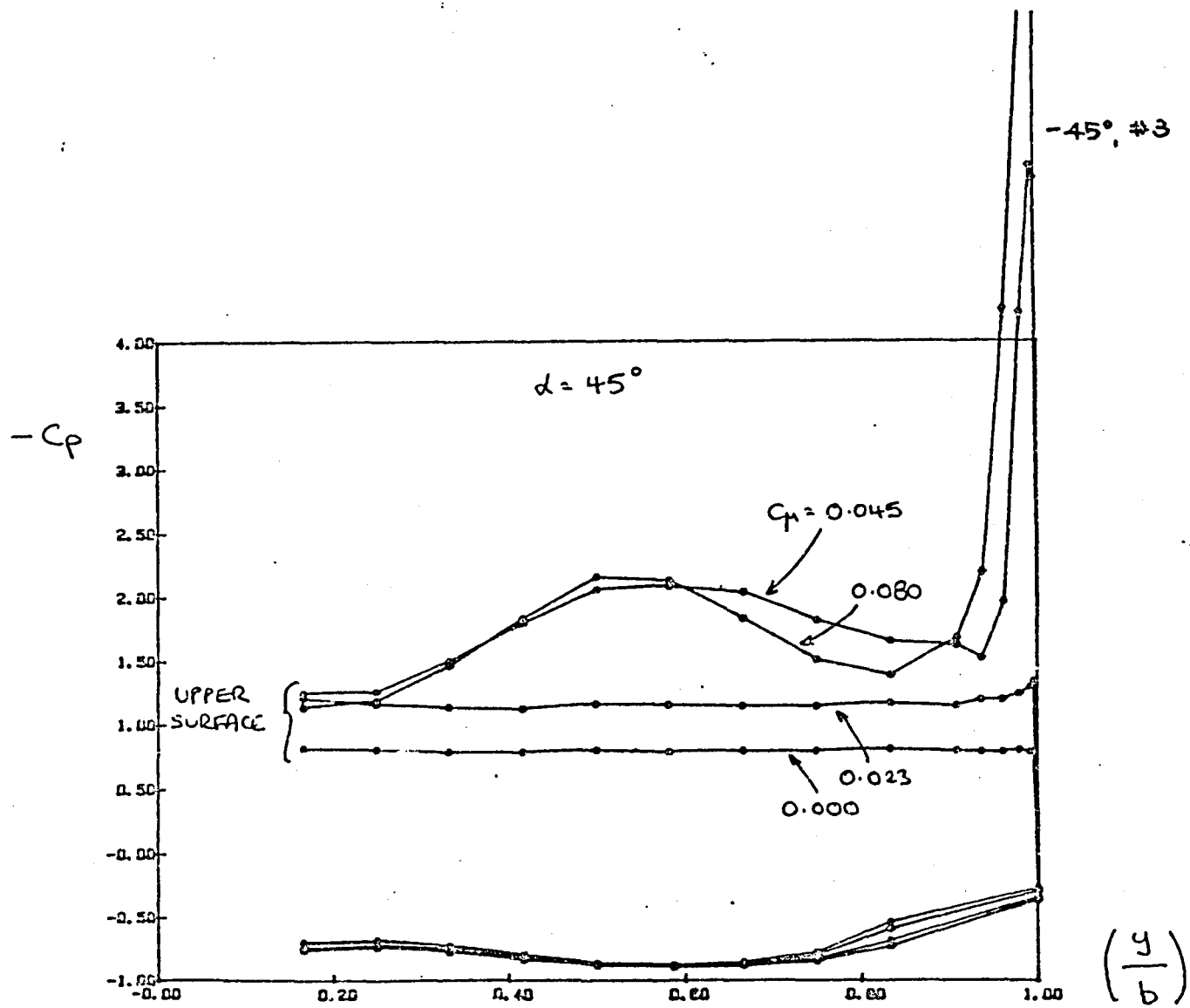

FIGURE 18a: PRESSURE DISTRIBUTION, ROW 3, CO-FLOWING CONFIGURATION

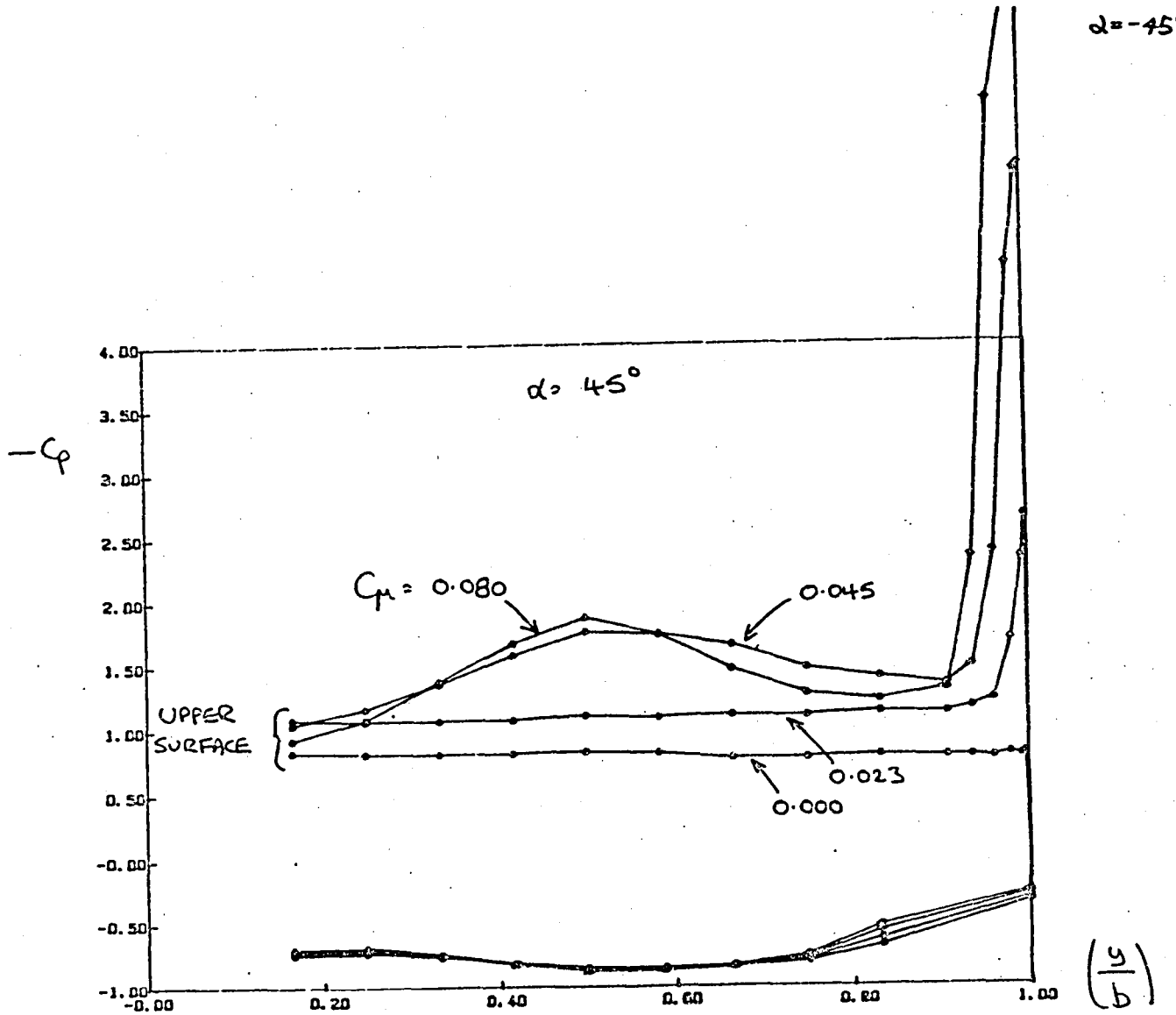

FIGURE 18 b: ROW 4

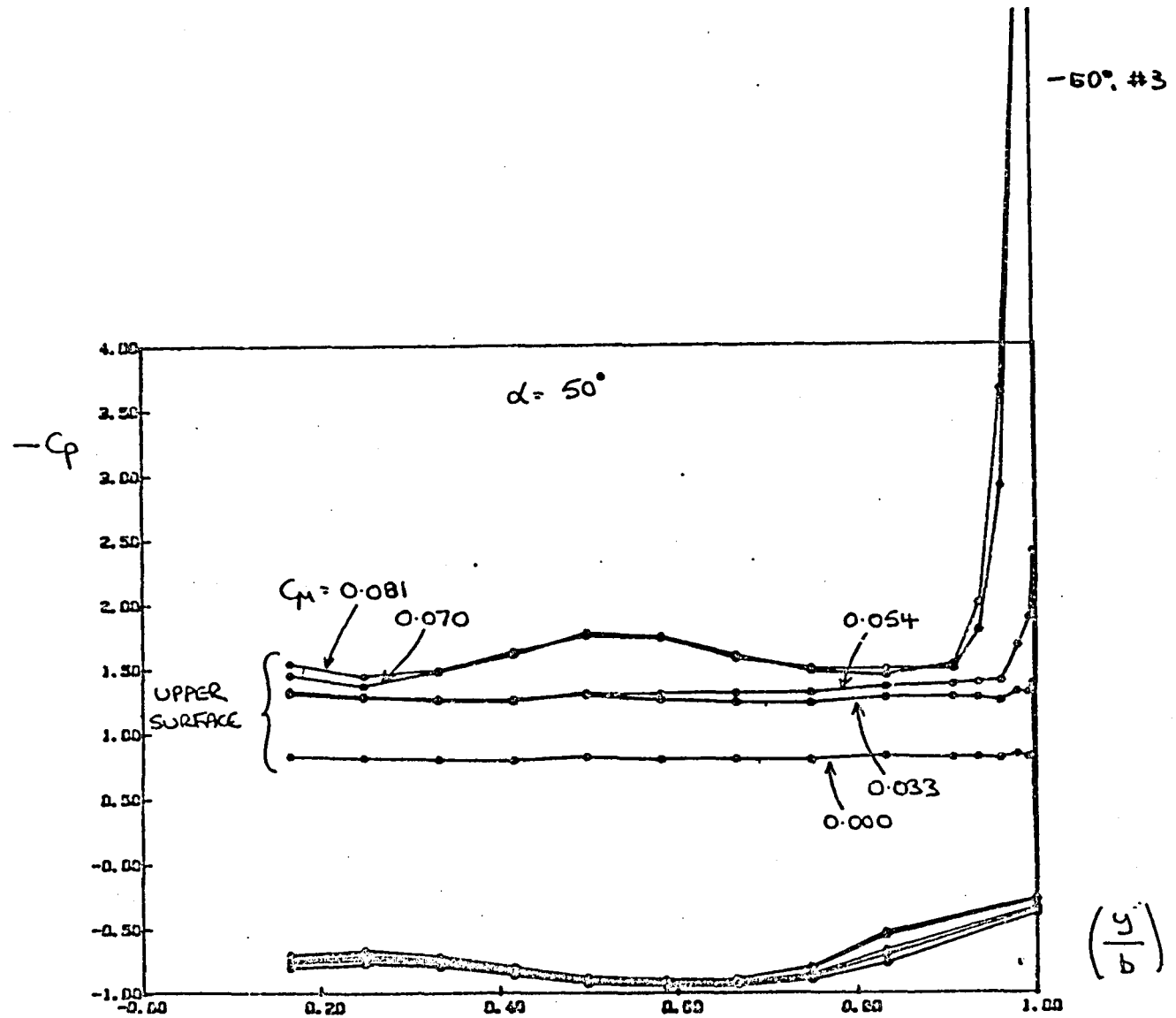

FIGURE 19a: PRESSURE DISTRIBUTION, ROW 3, CO-FLOWING CONFIGURATION

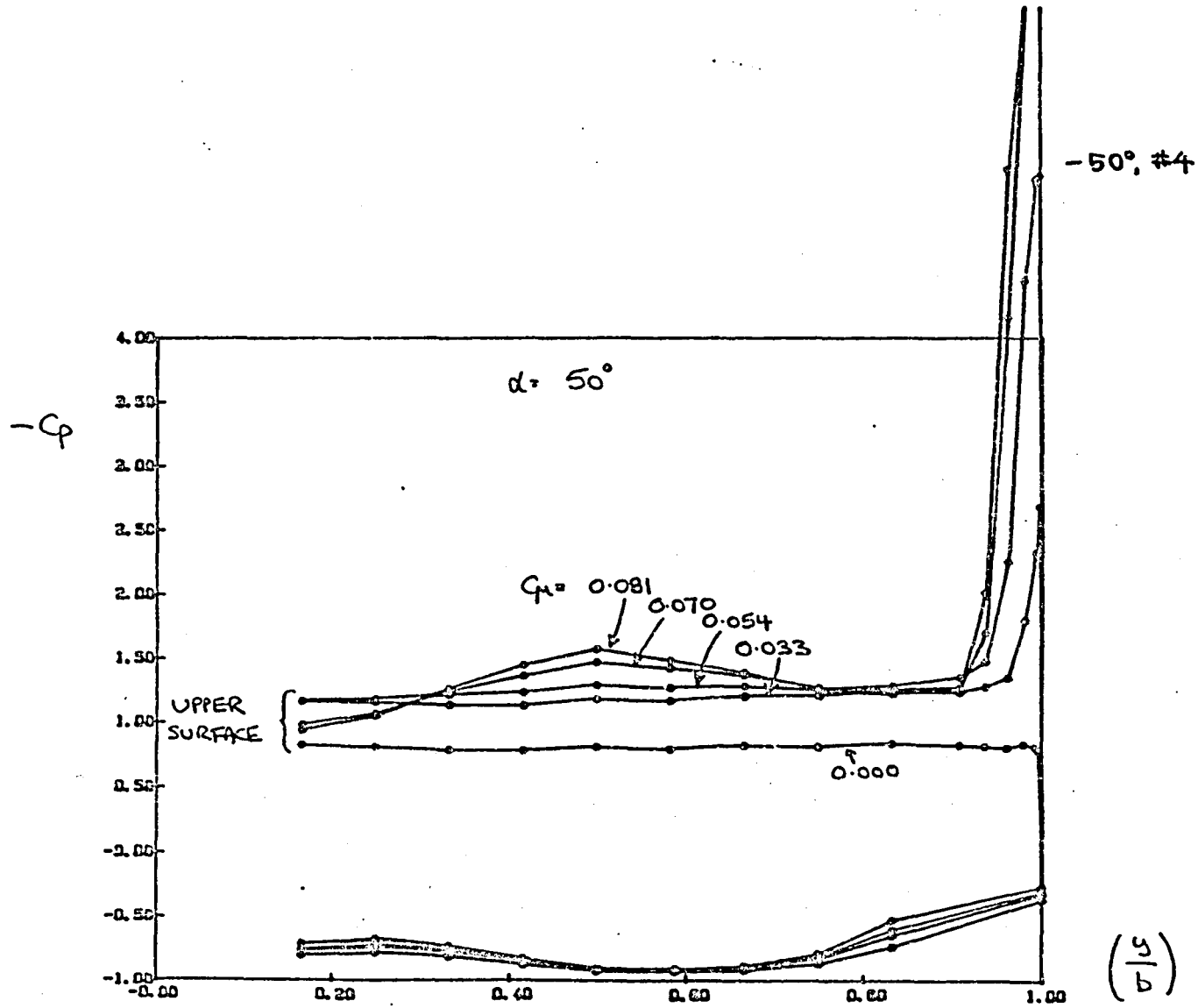

FIGURE 19b: ROW 4

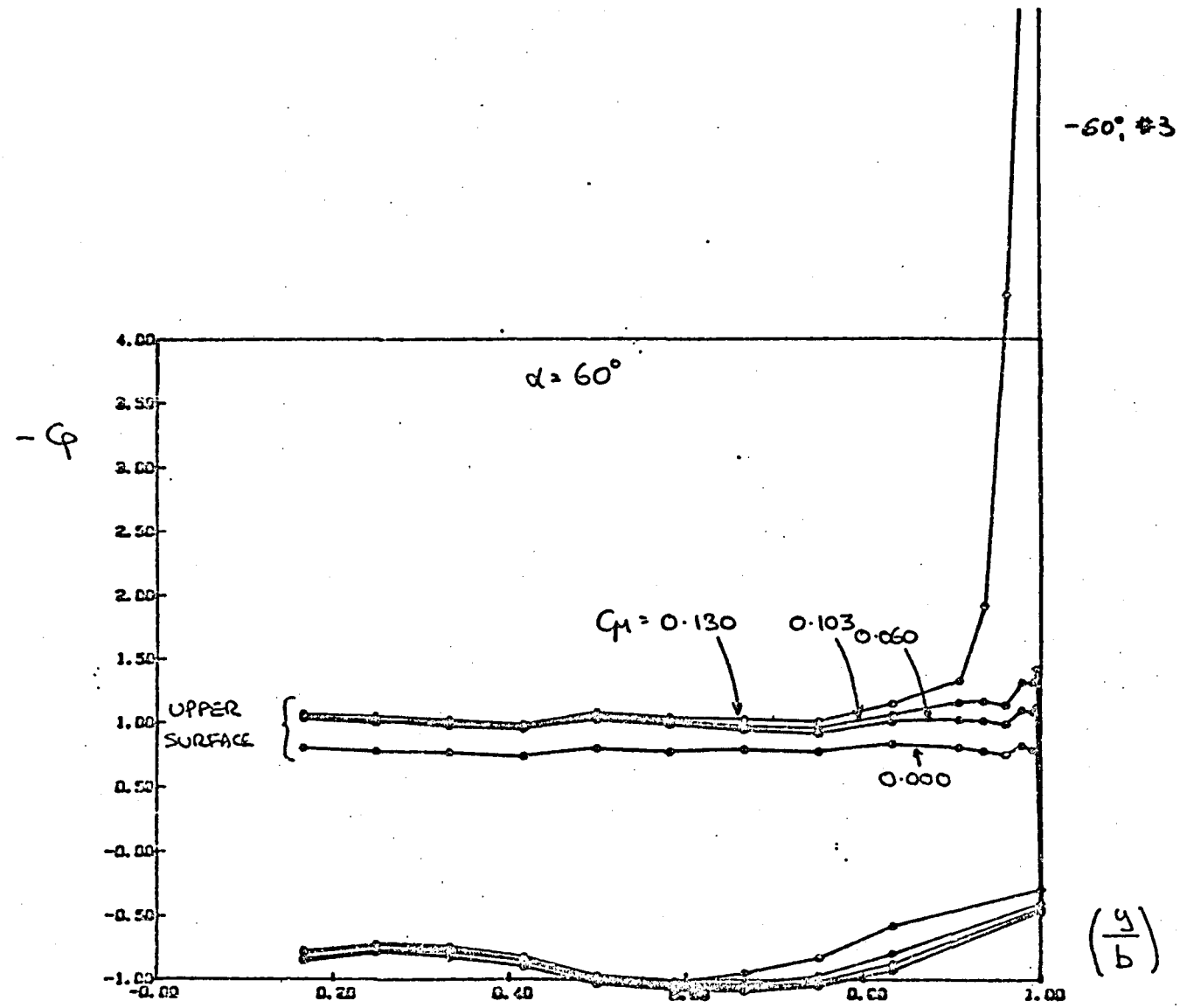

FIGURE 20 a: PRESSURE DISTRIBUTIONS, ROW 3, CO-FLOWING CONFIGURATION

ANGLE -60° (#4)

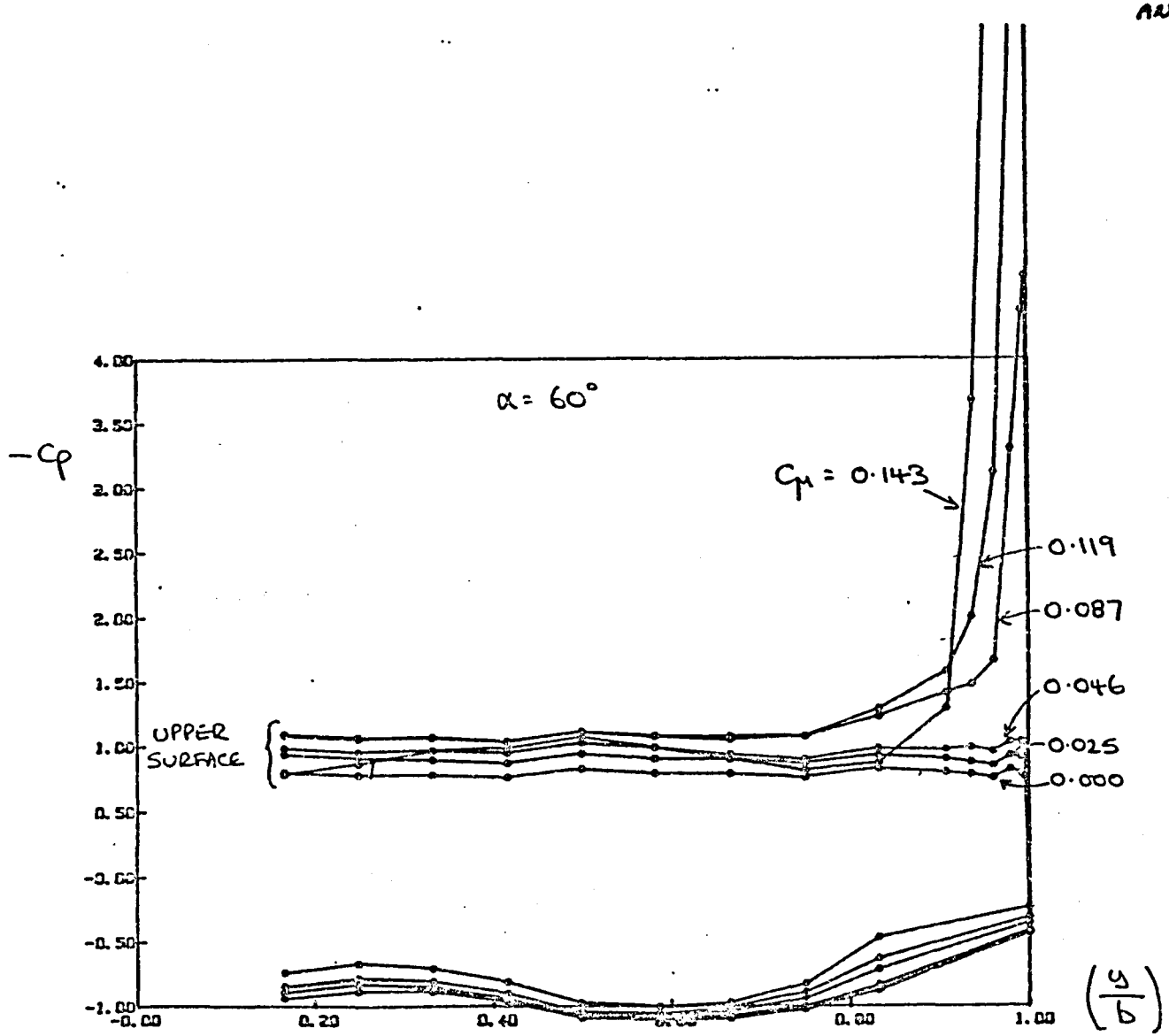

FIGURE 20 b: Row 4

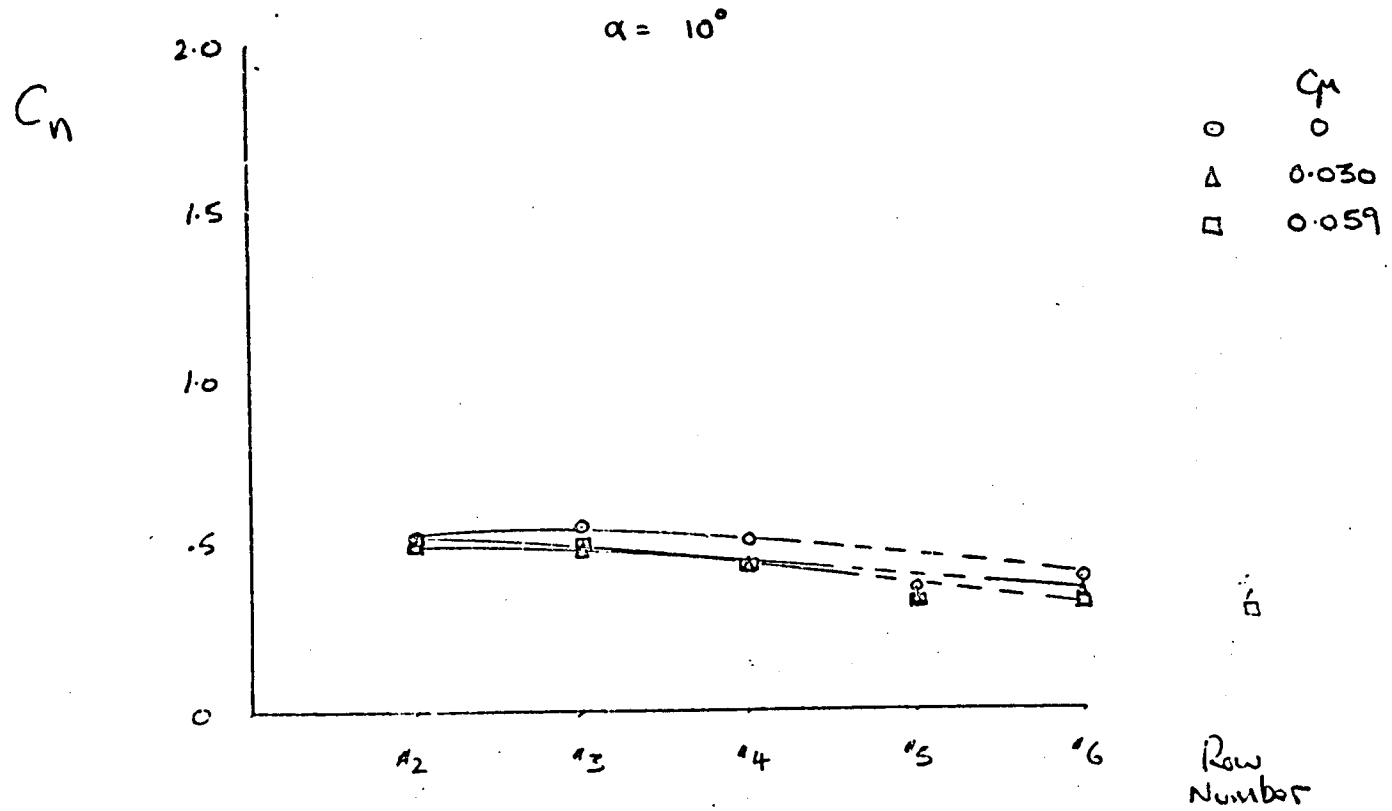

FIGURE 21a: LONGITUDINAL LOAD DISTRIBUTIONS, $\alpha = 10°$, COUNTER-FLOWING CONFIGURATION

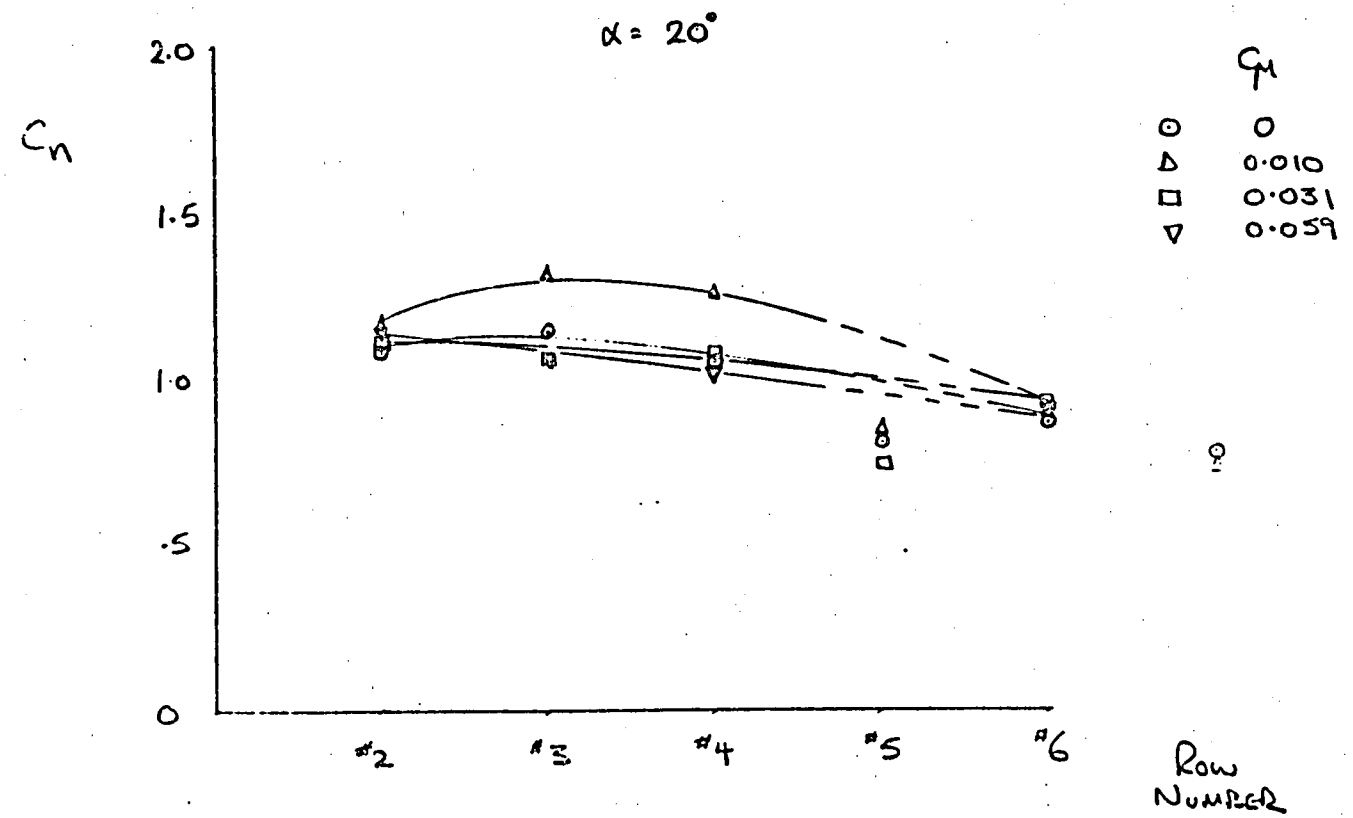

FIGURE 21b: $\alpha = 20°$

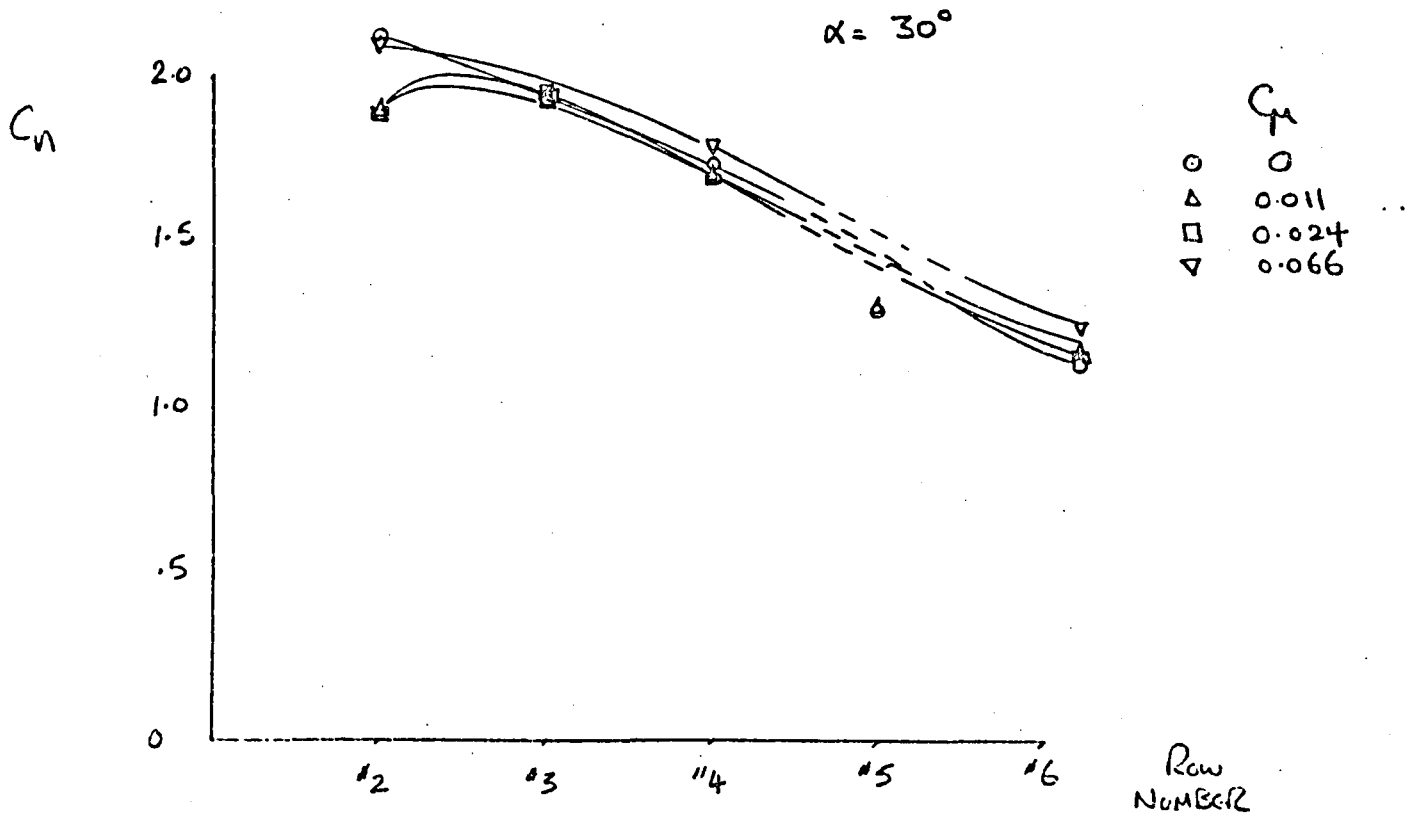

FIGURE 21 c: $\alpha = 30°$

10°, #3

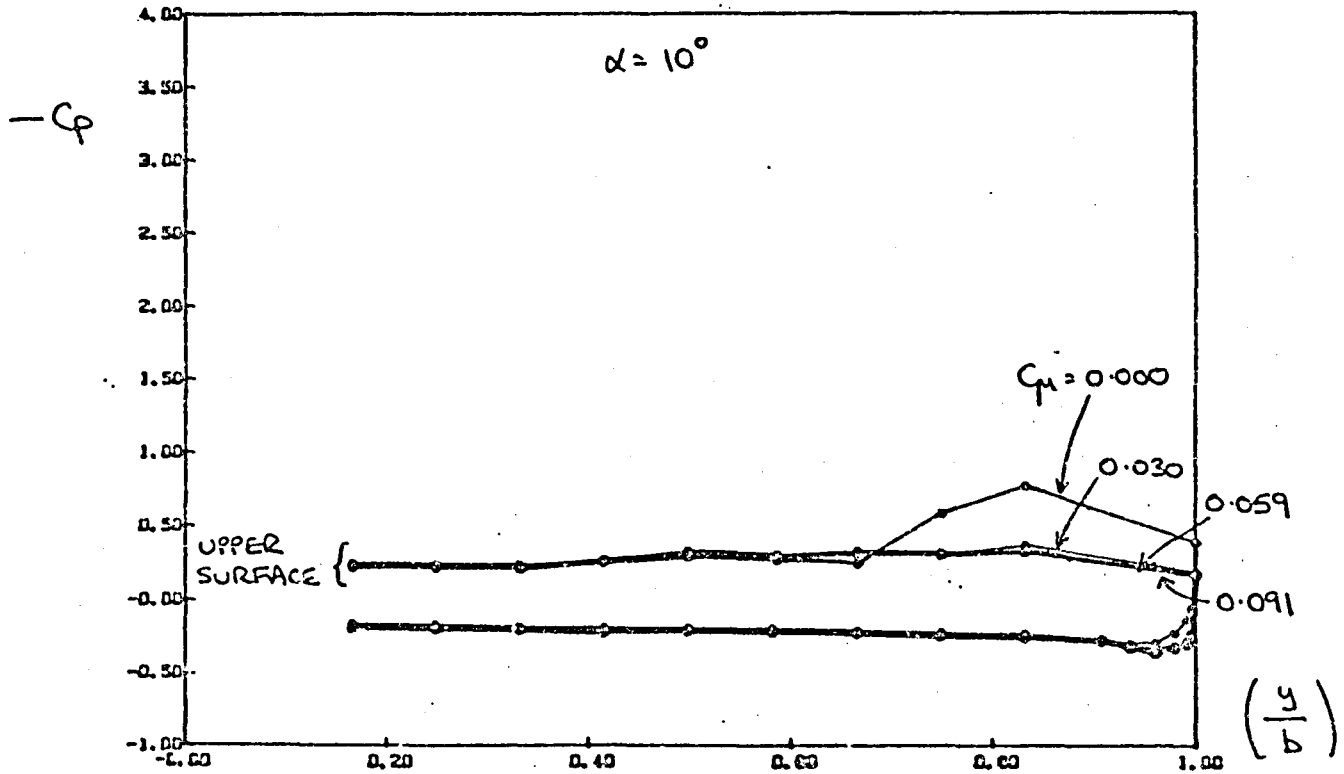

FIGURE 22a: PRESSURE DISTRIBUTIONS, ROW 3, COUNTER-FLOWING CONFIGURATION

ANGLE 10° (114)

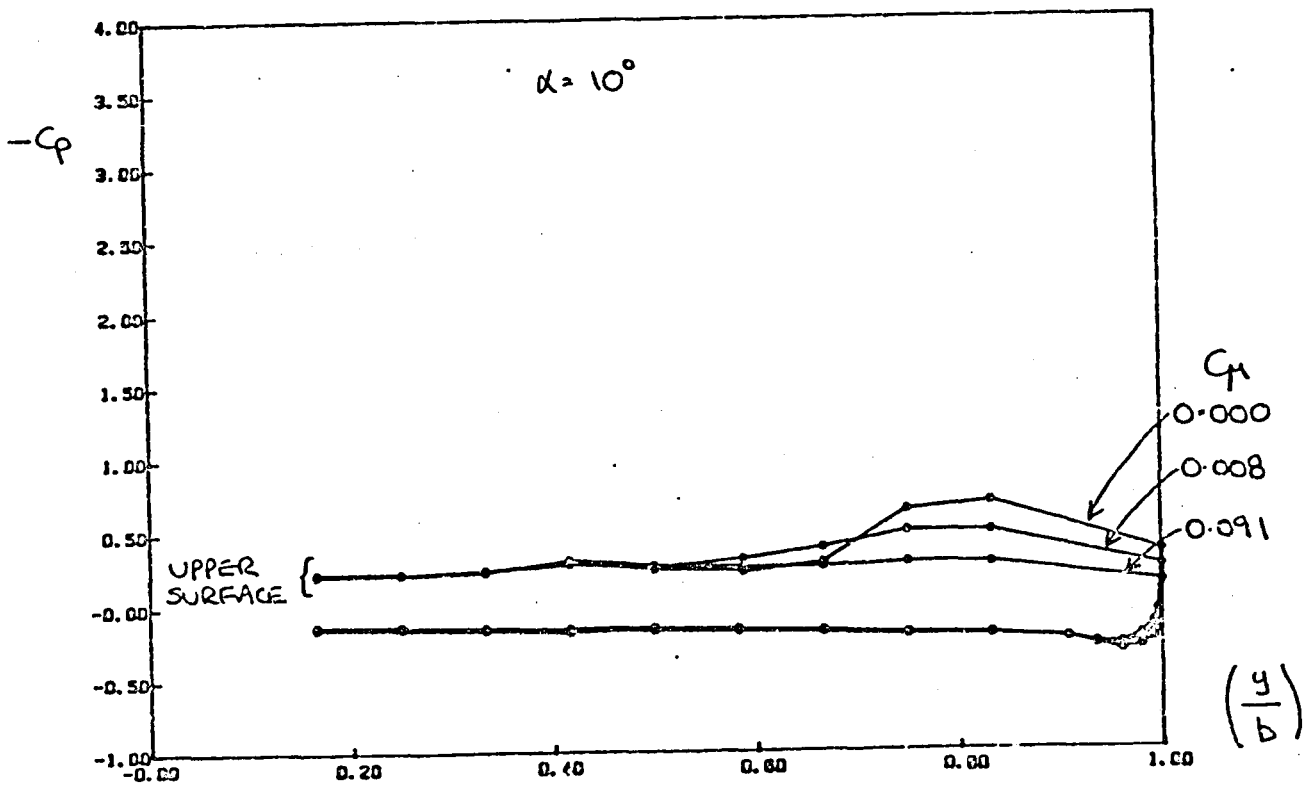

FIGURE 22 b: ROW 4

20°, #3
low C_μ

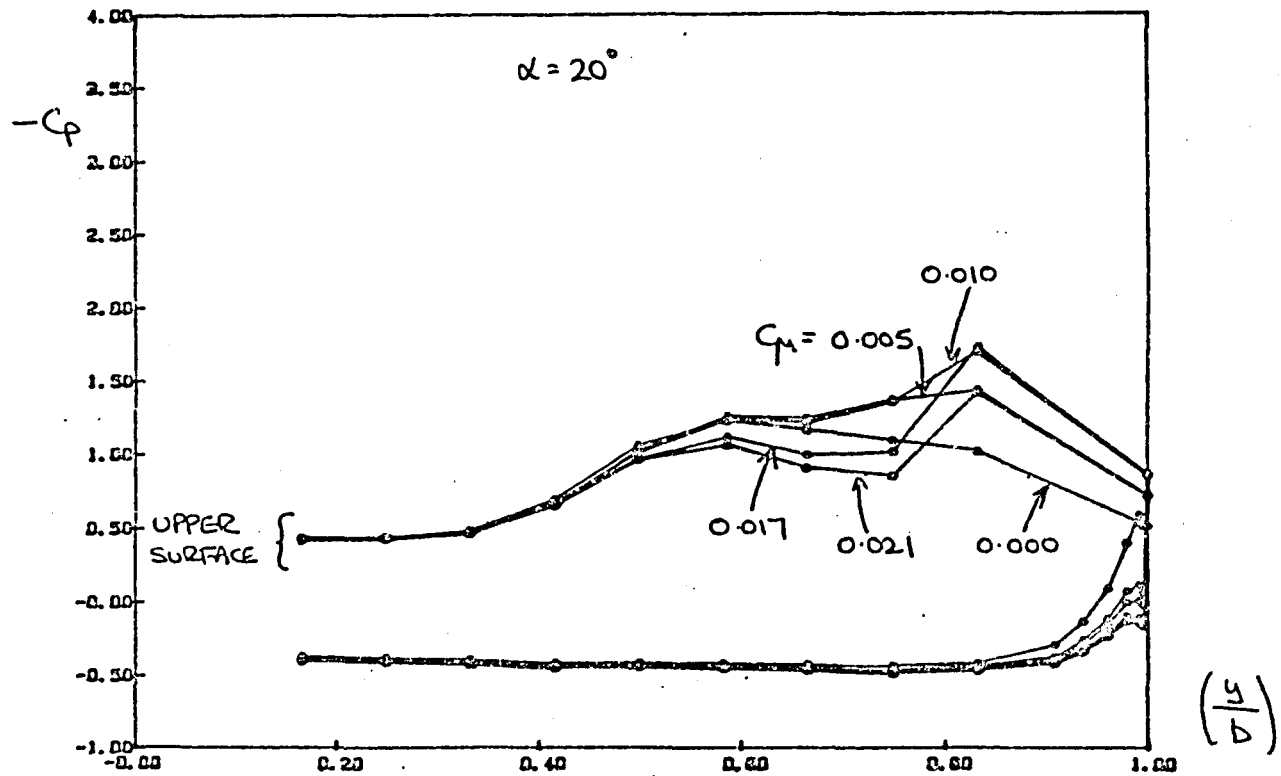

FIGURE 23a: PRESSURE DISTRIBUTIONS, ROW 3, COUNTER-FLOWING CONFIGURATION

20°, #4
low C_μ

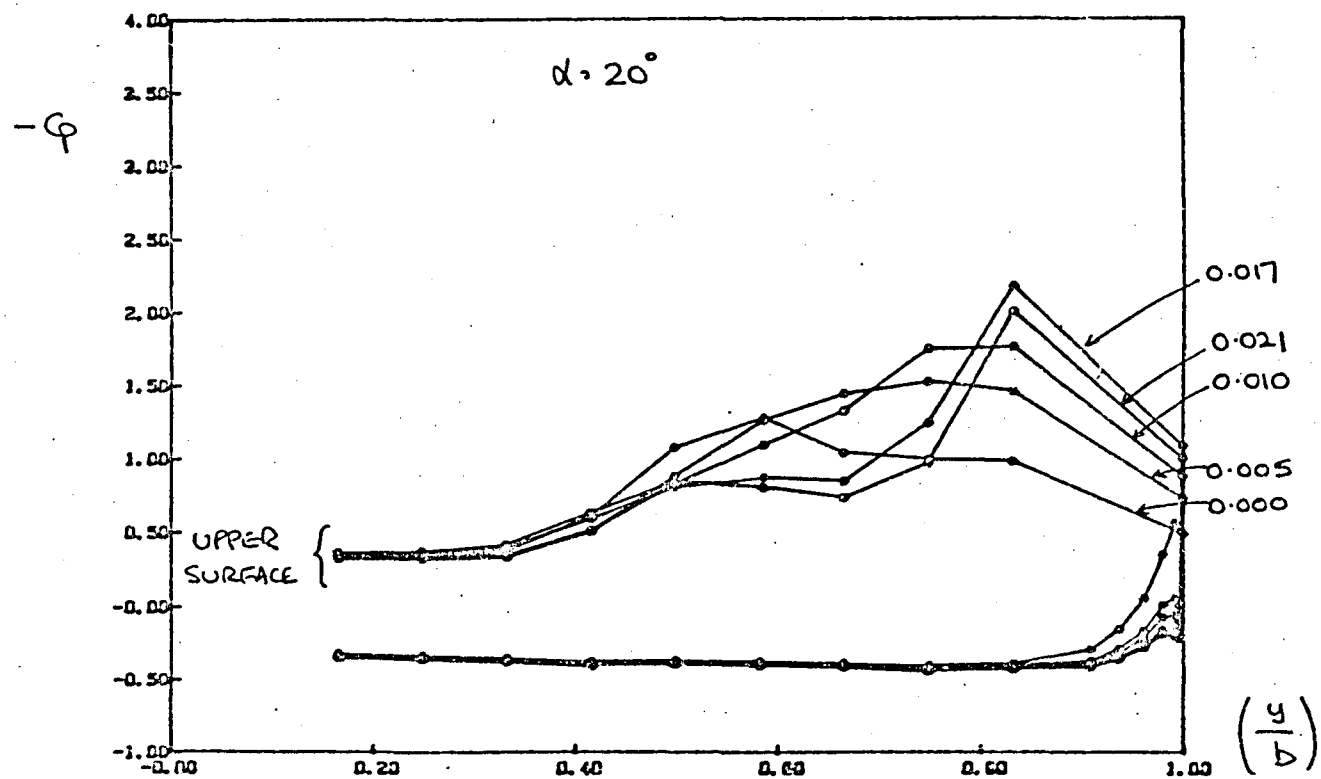

FIGURE 23 b: ROW 4

30°, #3

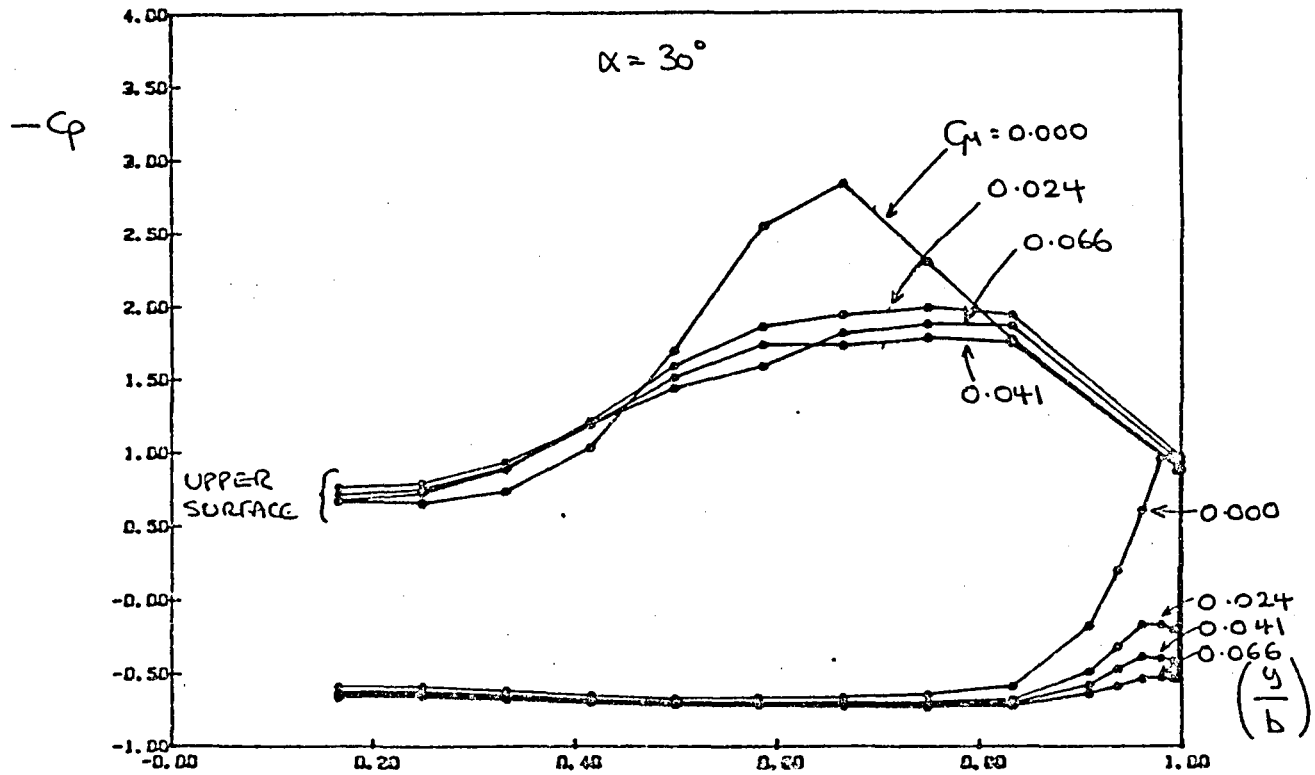

FIGURE 24a: PRESSURE DISTRIBUTIONS, ROW 3, COUNTER-FLOWING CONFIGURATION

30°

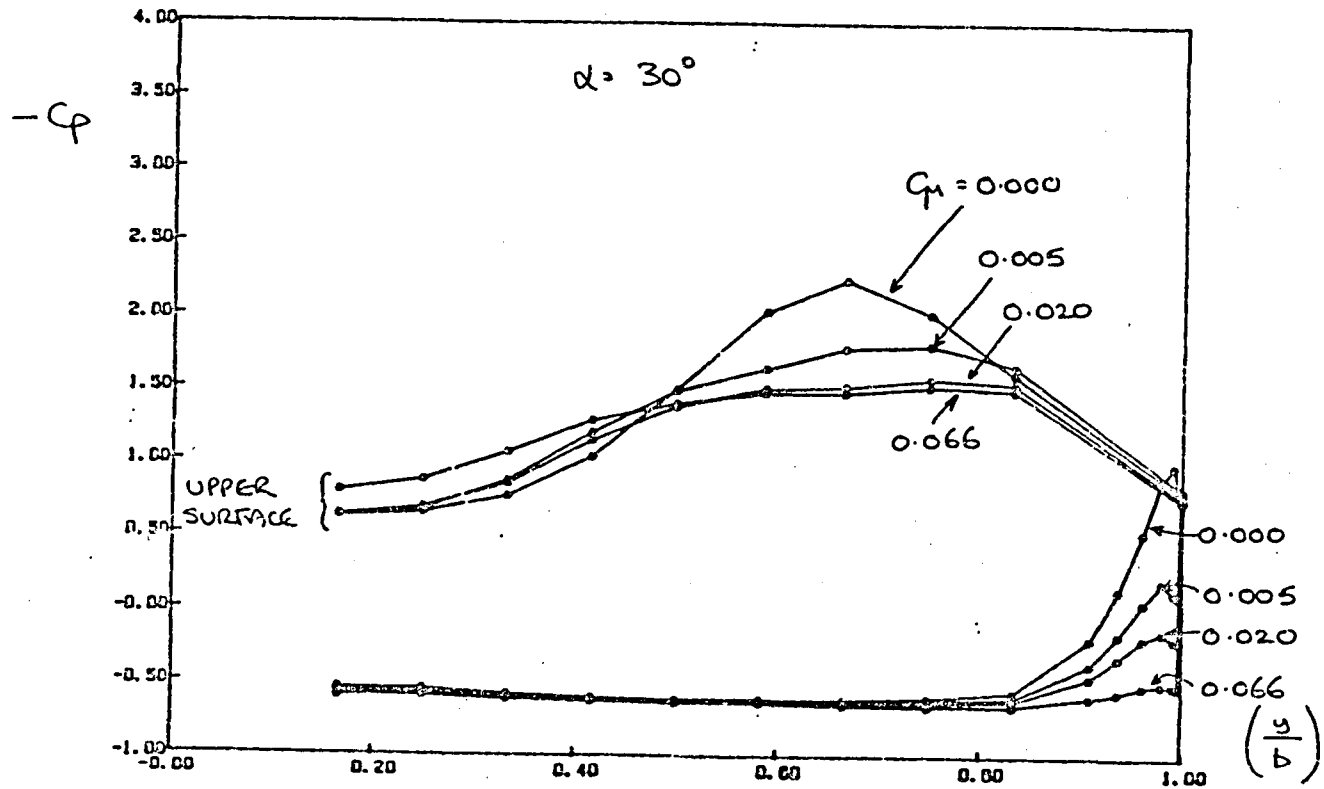

FIGURE 24b: ROW 4

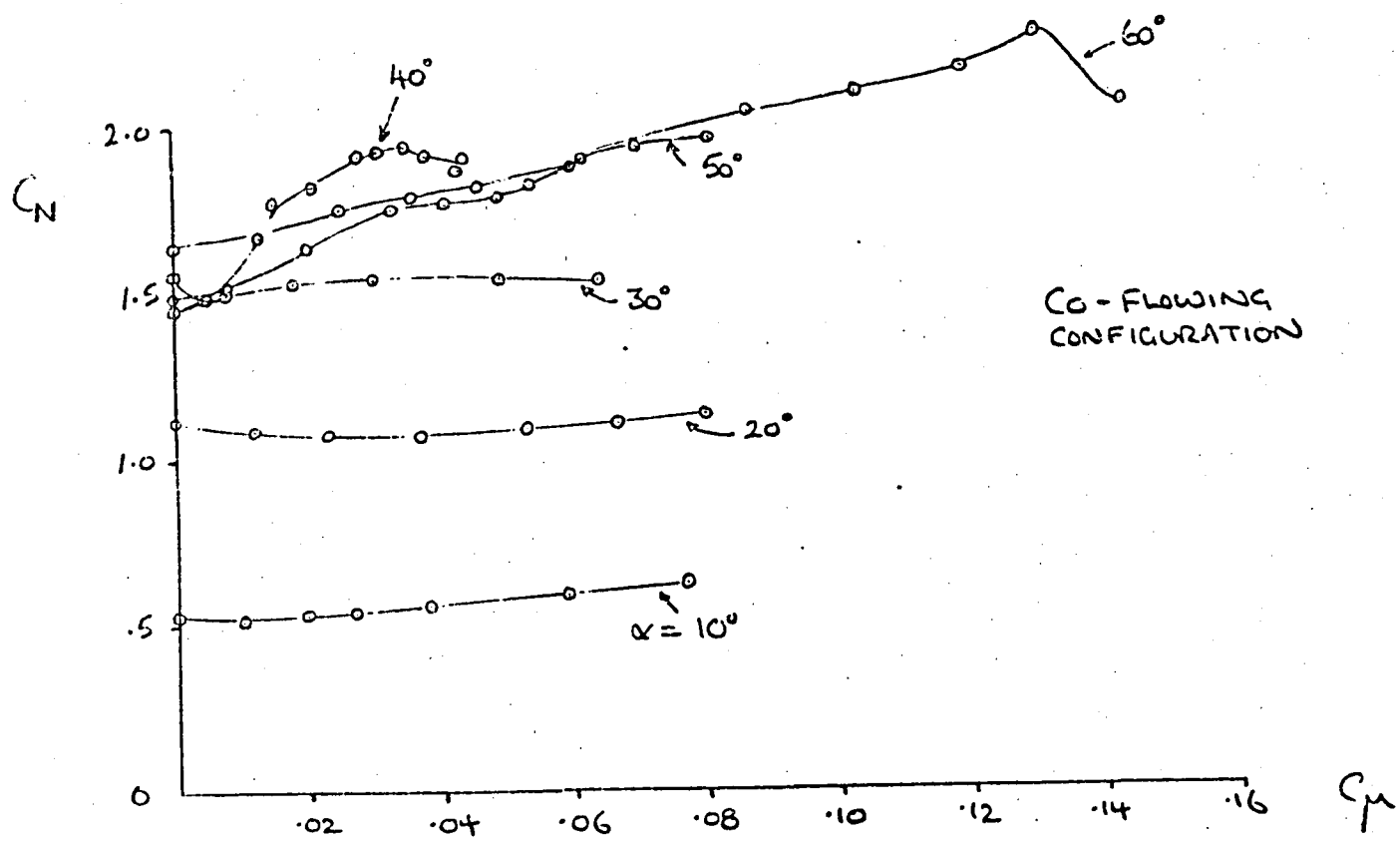

FIGURE 25a: GENERATION OF WING NORMAL FORCE BY BLOWING (FOR CONSTANT α)

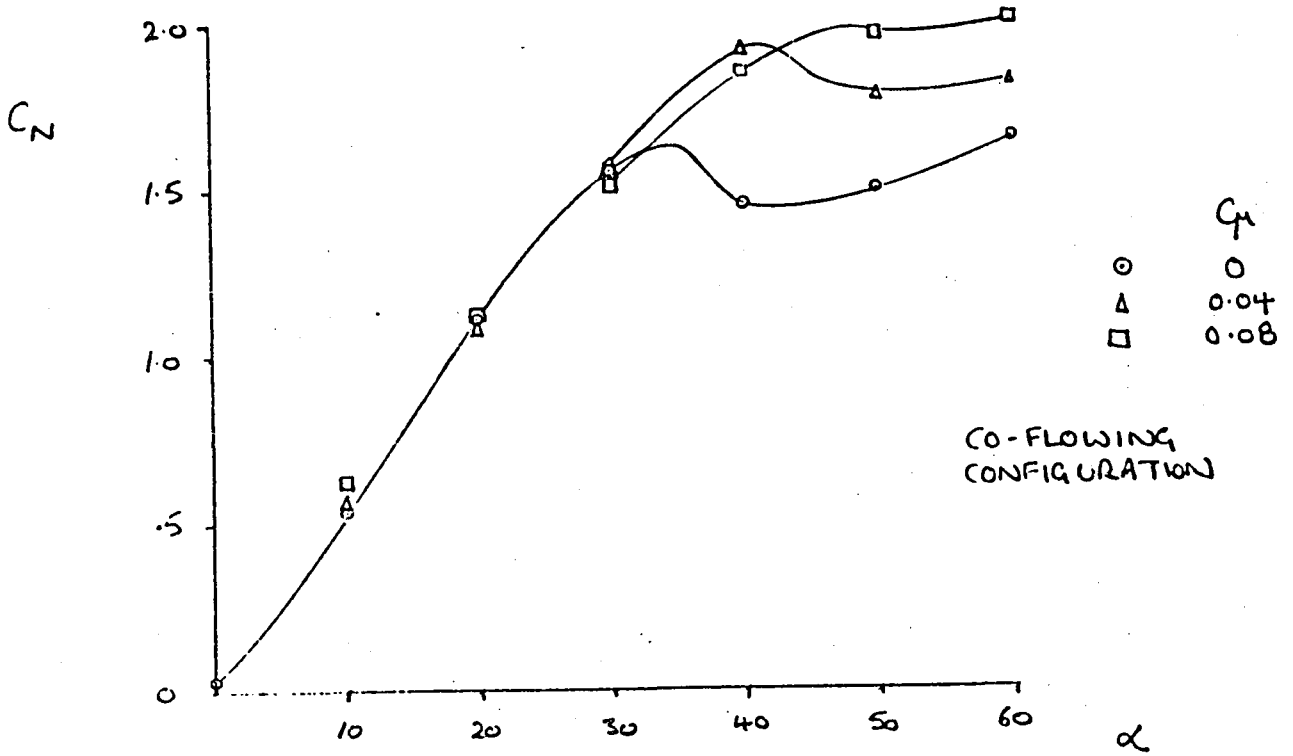

FIGURE 25b: GENERATION OF WING NORMAL FORCE FOR CONSTANT BLOWING

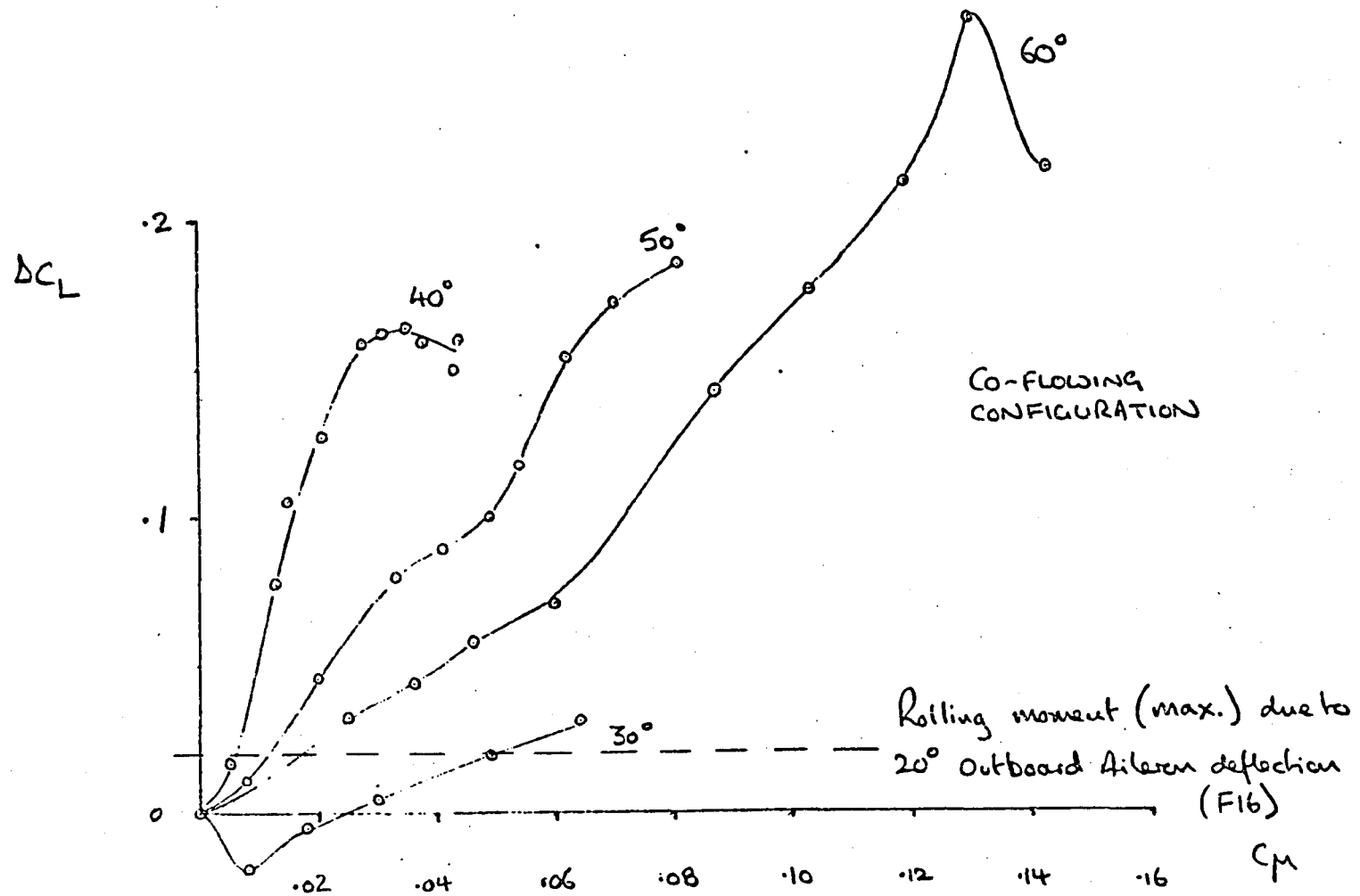

FIGURE 26: INCREMENTAL ROLLING MOMENT PRODUCED BY BLOWING

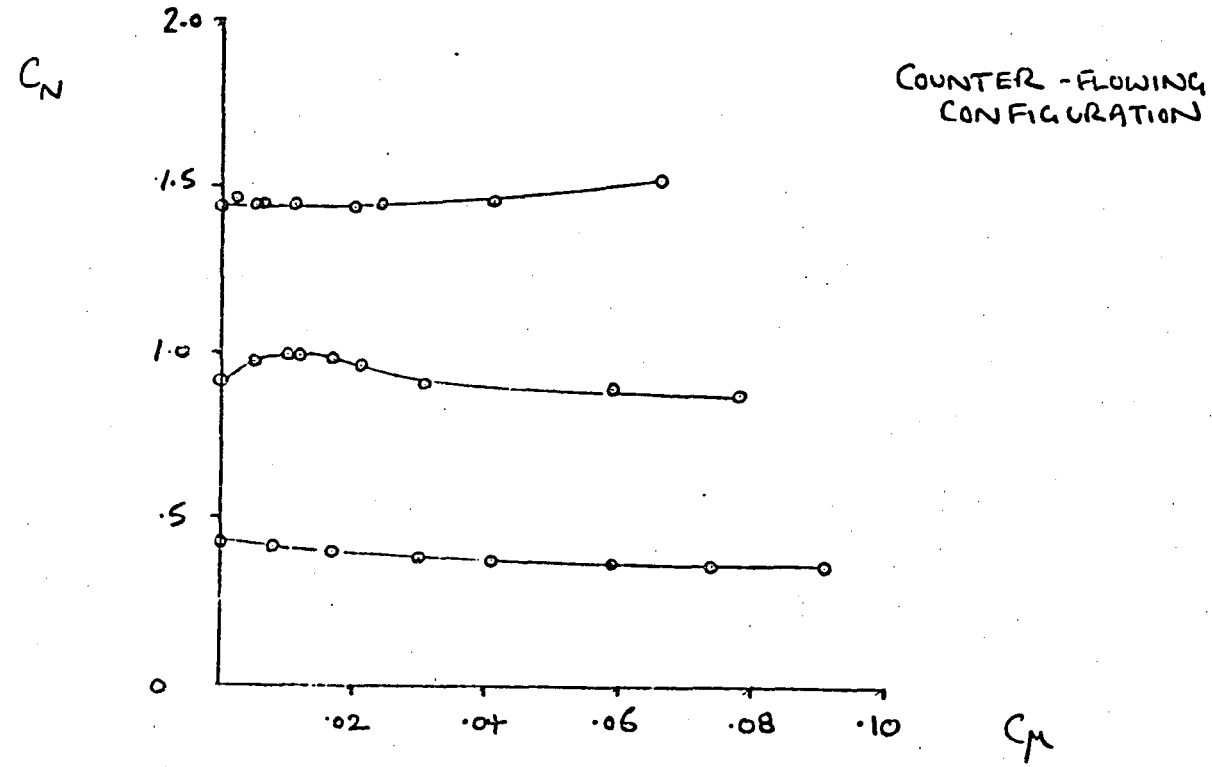

FIGURE 27: GENERATION OF WING NORMAL FORCE BY BLOWING

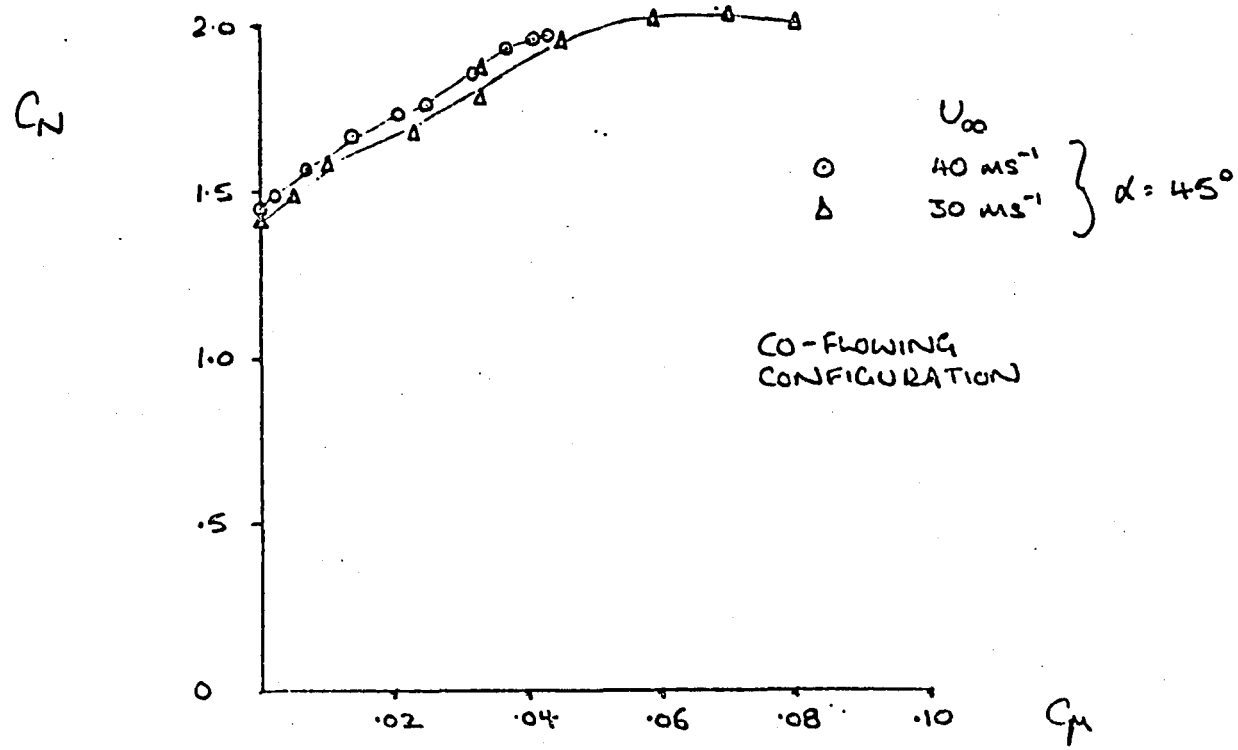

FIGURE 28: EFFECT OF REYNOLDS NUMBER ON THE PRODUCTION OF WING NORMAL FORCE BY BLOWING

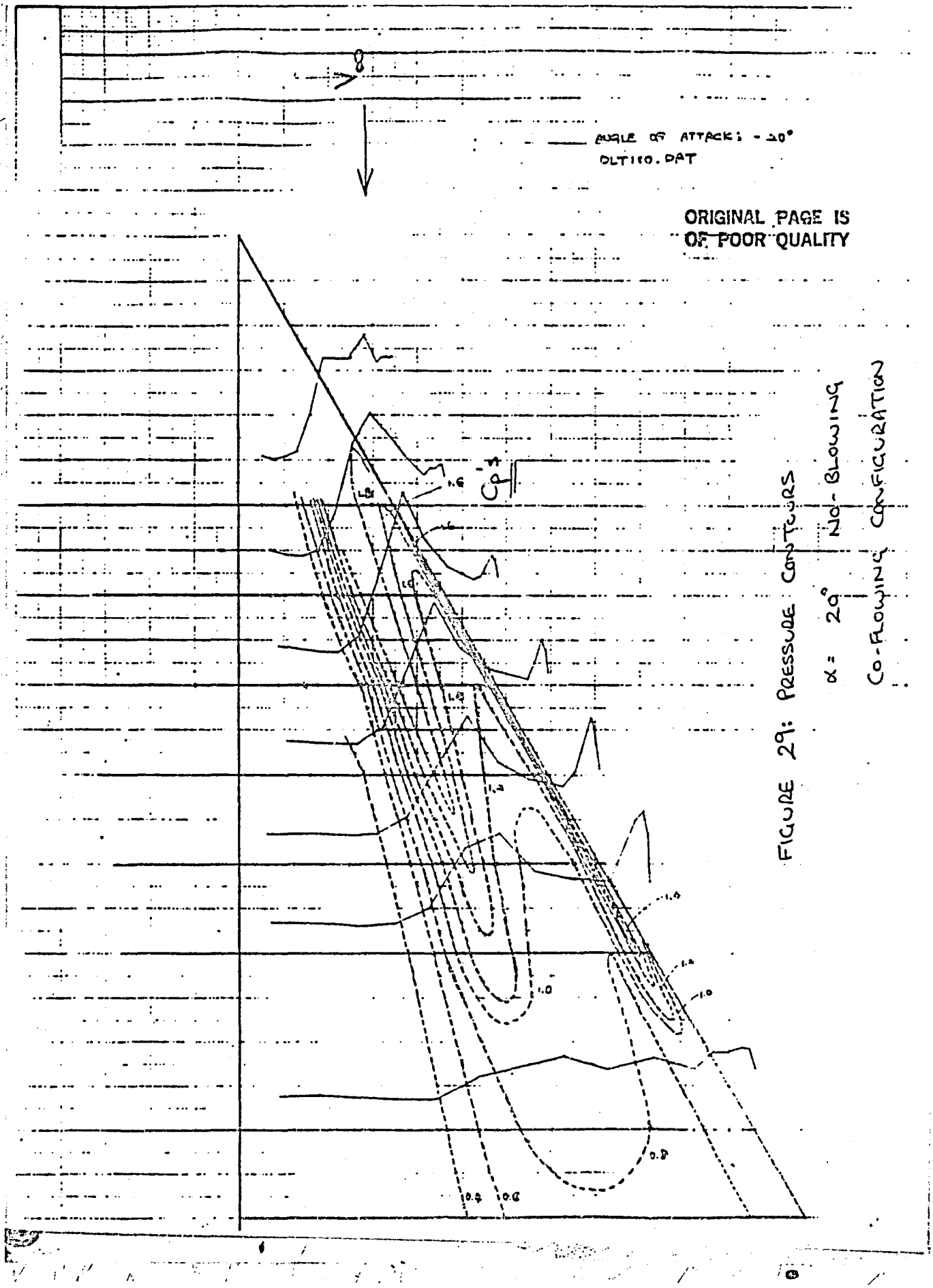

FIGURE 29: PRESSURE CONTOURS
$\alpha = 20°$ NO-BLOWING
CO-FLOWING CONFIGURATION

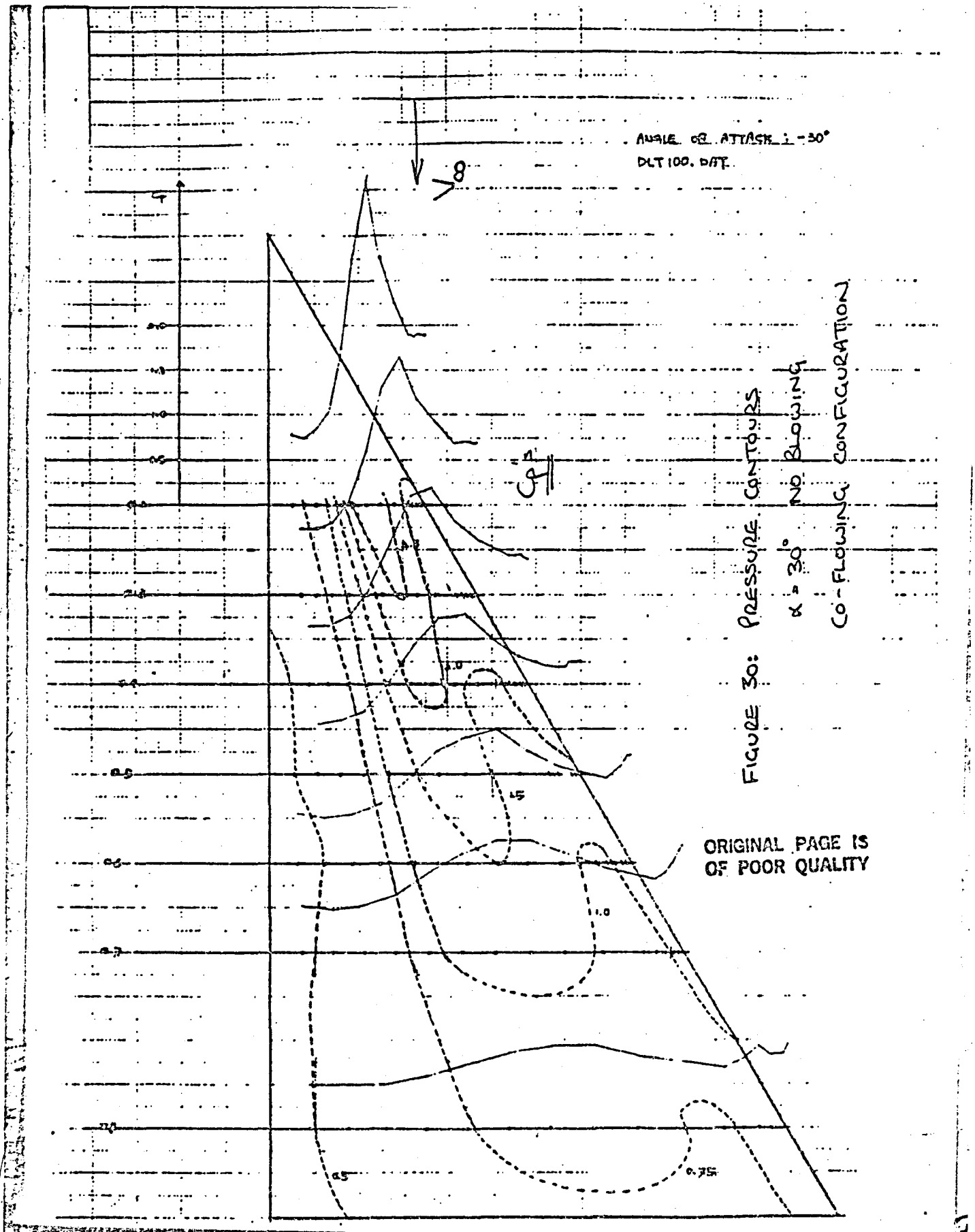

FIGURE 30: PRESSURE CONTOURS $\alpha = 30°$ NO BLOWING CO-FLOWING CONFIGURATION

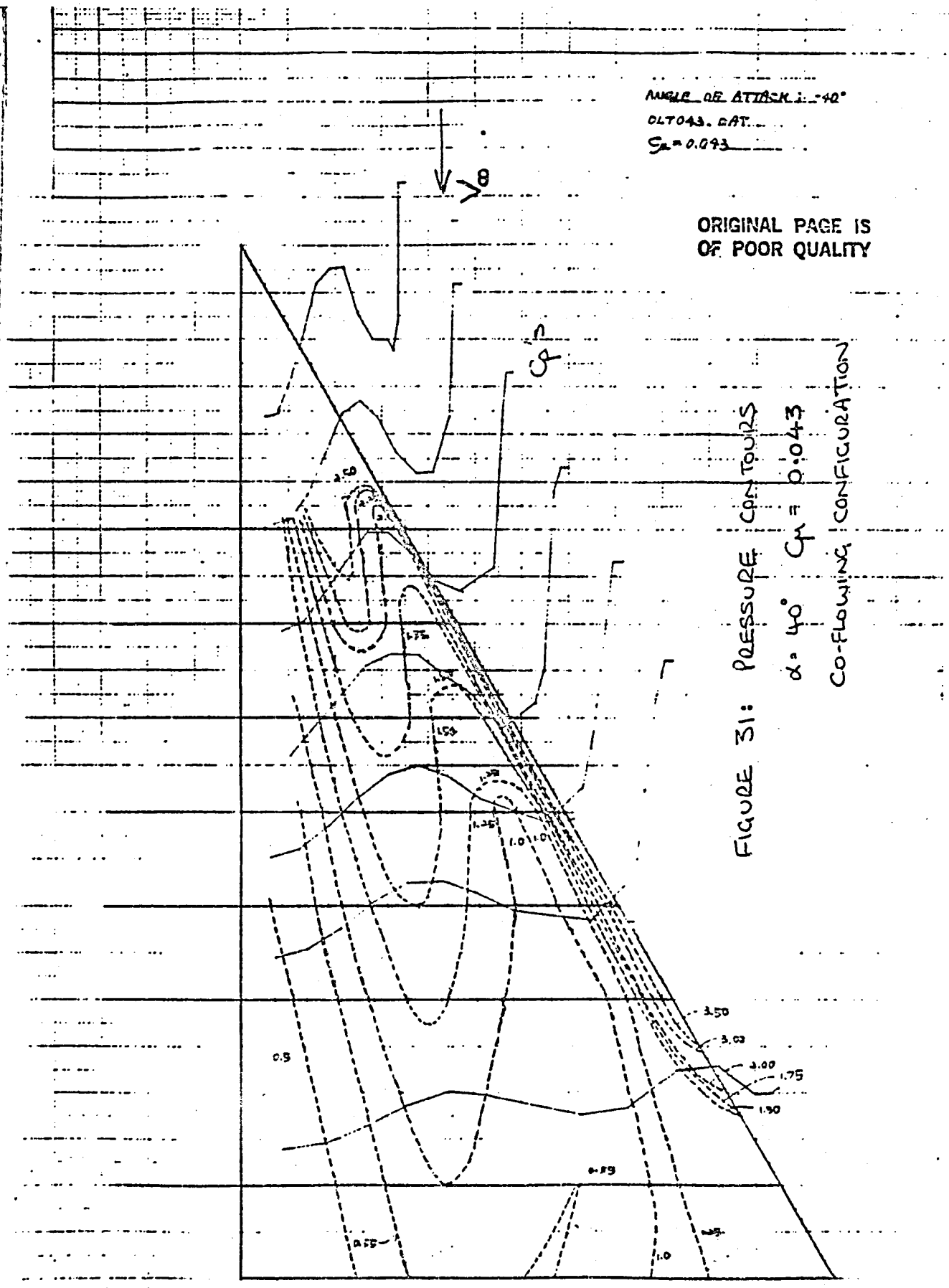

ORIGINAL PAGE IS
OF POOR QUALITY

FIGURE 31: PRESSURE C_p CONTOURS
α = 40° C_μ = 0.043
CO-FLOWING CONFIGURATION

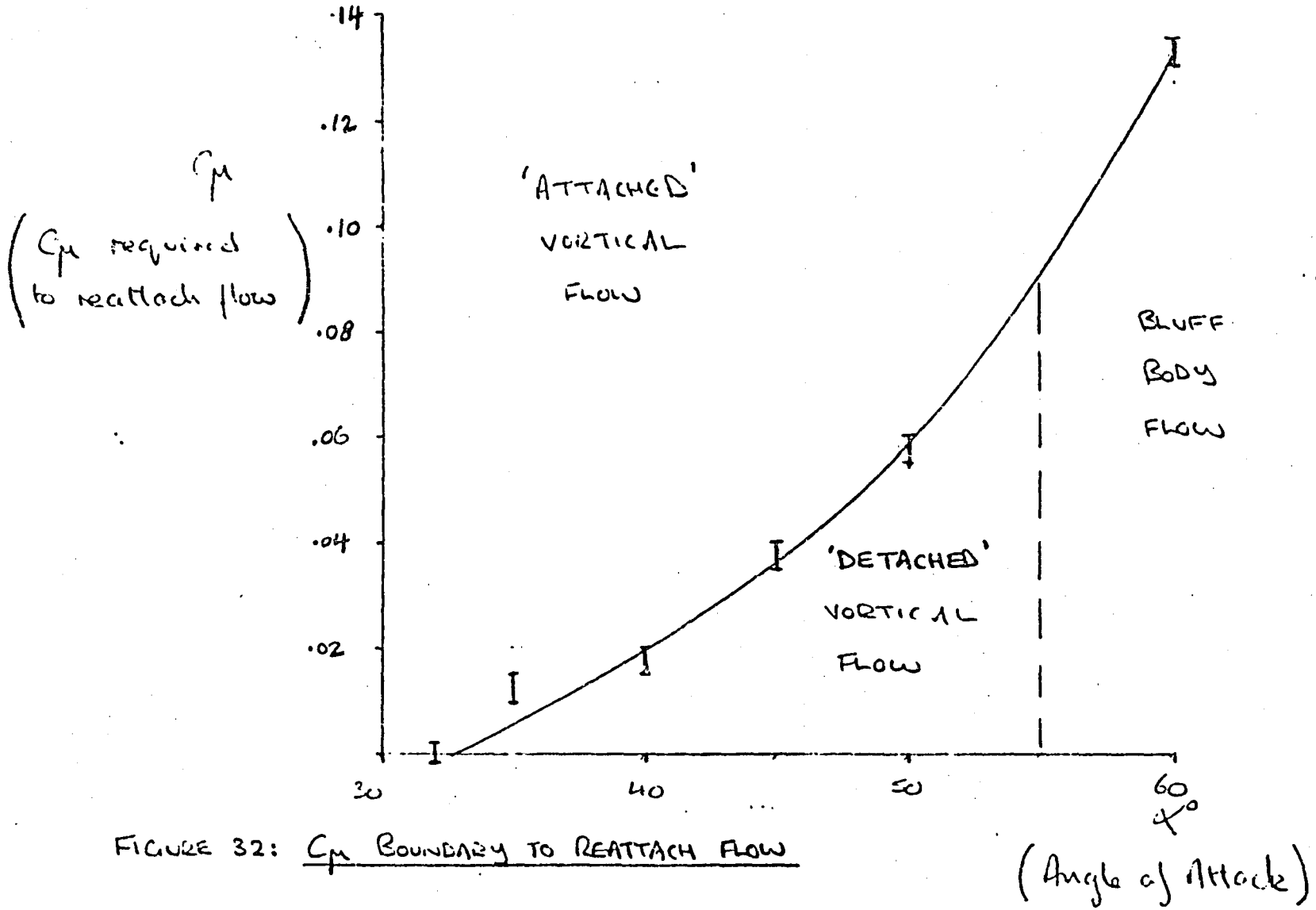

FIGURE 32: C_μ BOUNDARY TO REATTACH FLOW

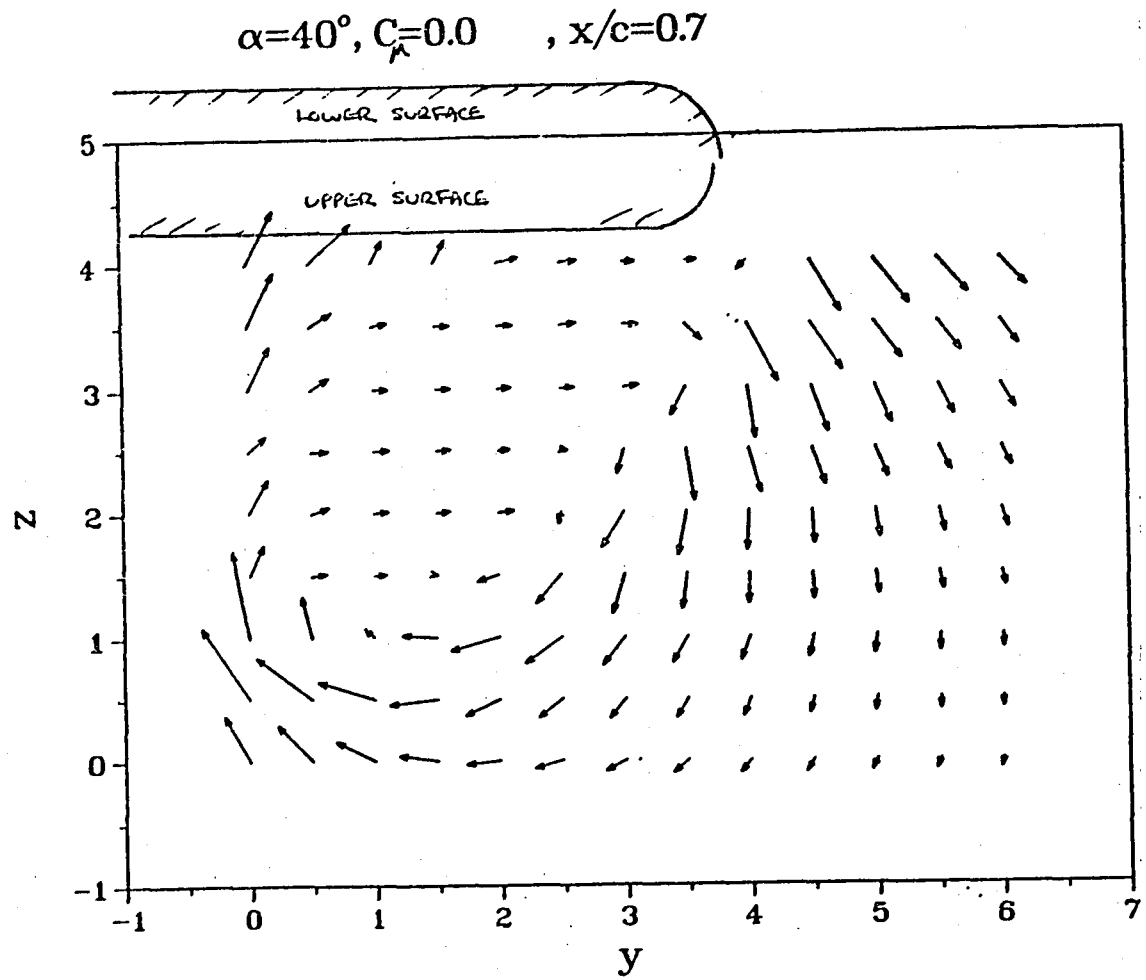

FIGURE 33: CROSS-FLOW MAPPING, $\alpha = 40$, NO-BLOWING, CO-FLOWING CONFIGURATION

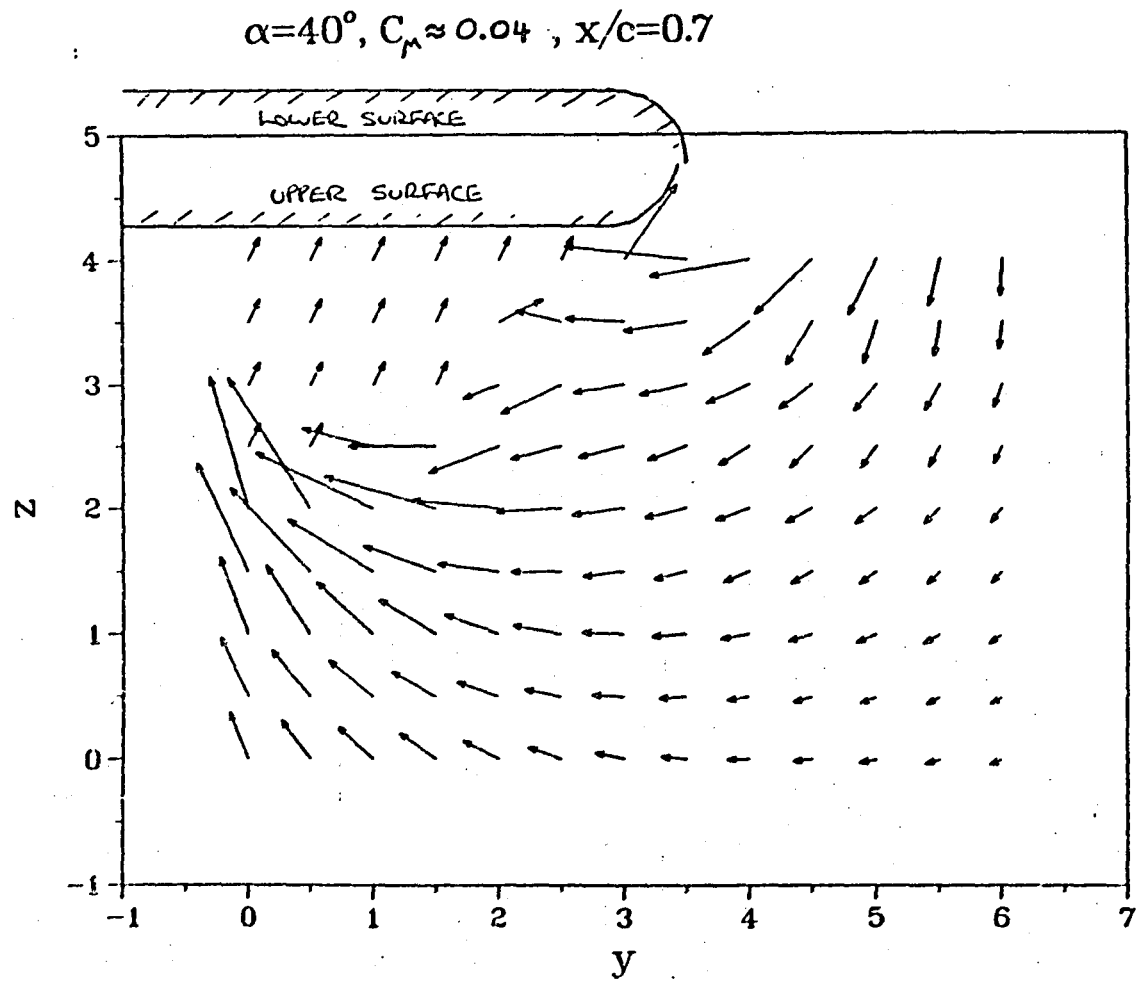

FIGURE 34: CROSS FLOW MAPPING , $\alpha = 40$, $C_\mu \approx 0.040$, CO-FLOWING CONFIGURATION

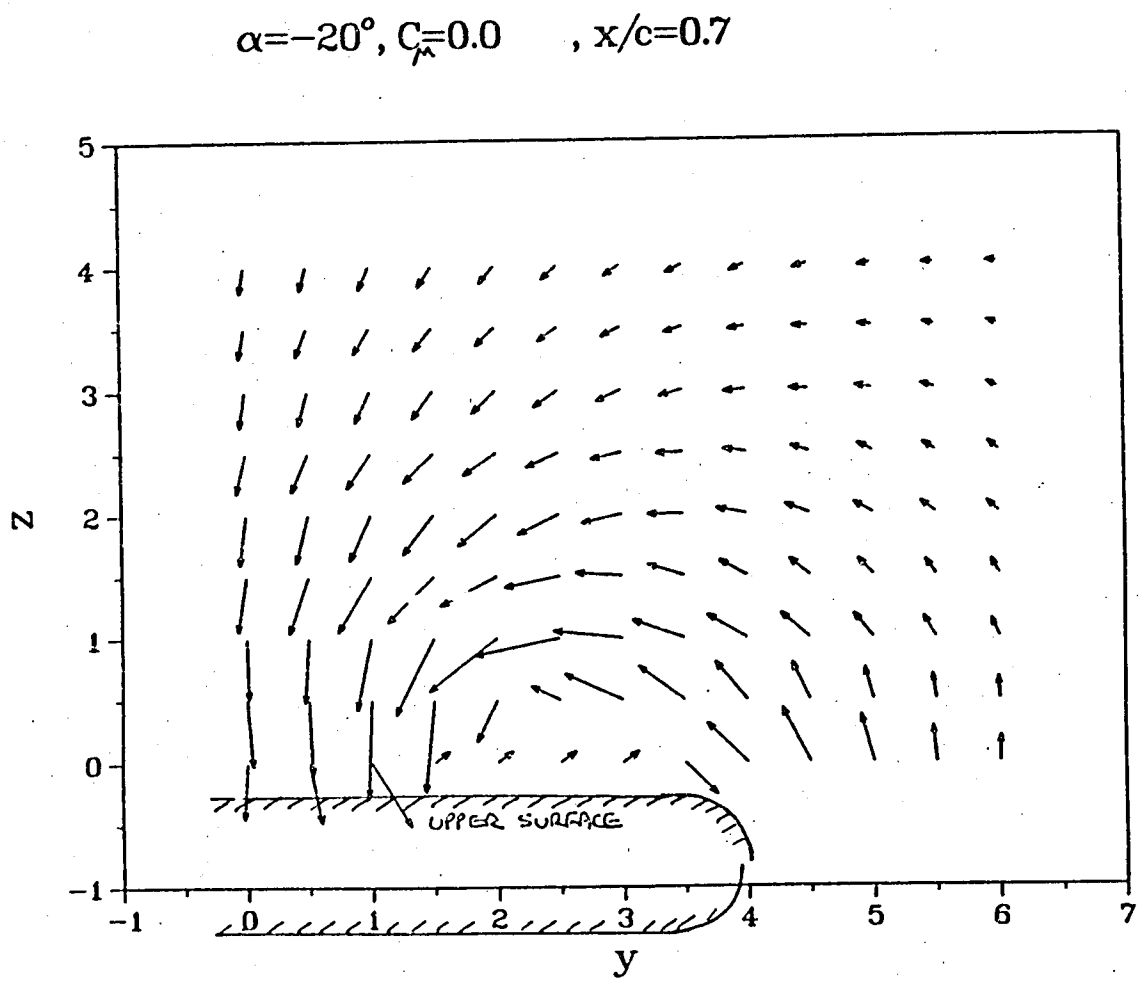

FIGURE 35: CROSS FLOW MAPPING, $\alpha = 20$, NO-BLOWING, COUNTER-FLOW CONFIGURATION

$\alpha = -20°$, $C_M \approx 0.005$., $x/c = 0.7$

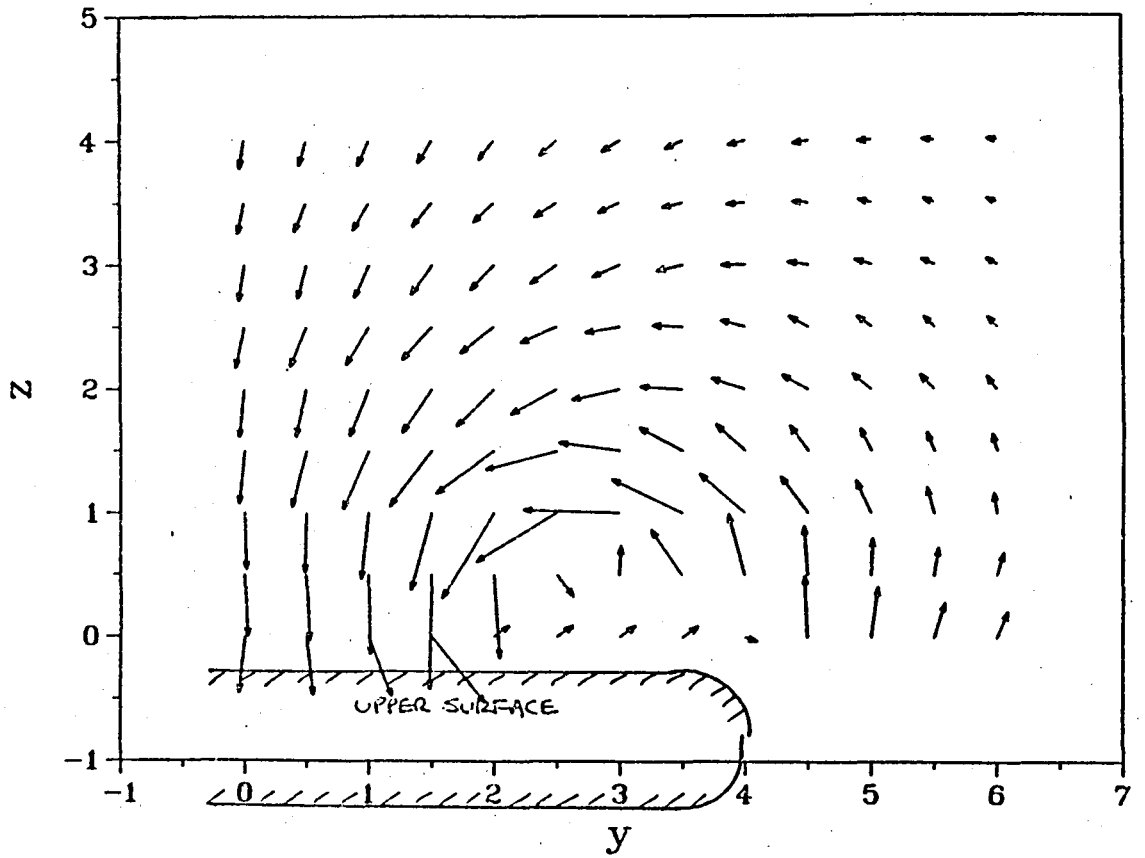

FIGURE 36: CROSS FLOW MAPPING, $\alpha = 20$, $C_M \approx 0.005$, COUNTER-FLOW CONFIGURATION

END

DATE

FILMED

OCT 9 1986

End of Document